Energy Conversion and Management 343 (2025) 120067

Contents lists available at ScienceDirect

Energy Conversion and Management

journal homepage: www.elsevier.com/locate/enconman

Research paper

Computer-aided molecular design of diffusion–absorption refrigeration modules for low-temperature solar collectors

Asmaa A. Harraz [a,b], Andrew J. Haslam [a,c], Niall Mac Dowell [a,d], Christos N. Markides [a,*]

[a] Clean Energy Processes (CEP) Laboratory & The Sargent Centre for Process Systems Engineering, Department of Chemical Engineering, Imperial College London, South Kensington Campus, London SW7 2AZ, UK
[b] Department of Chemical Engineering, Faculty of Engineering, Alexandria University, Alexandria 21544, Egypt
[c] Institute for Molecular Science and Engineering, Imperial College London, South Kensington Campus, London, SW7 2AZ, UK
[d] Centre for Environmental Policy, Imperial College London, South Kensington Campus, London, SW7 2AZ, UK

ARTICLE INFO

Keywords:
Computer-aided molecular design
CAMD
Diffusion absorption refrigeration
DAR
SAFT-γ Mie
Solar cooling

ABSTRACT

Diffusion absorption refrigeration (DAR) is an attractive thermally-driven cooling technology that can be powered using renewable heat, *e.g.*, from solar-thermal collectors. This technology can address refrigeration security challenges, rising electricity costs, as well as energy, resource-use and emissions concerns. Commercial DAR modules typically use NH_3—H_2O as the working fluid pair, which requires temperatures above 150 °C to be supplied to initiate cooling. Due to their lower saturation temperatures, organic working fluids can be attractive substitutes in enabling DAR modules to be used in conjunction with low-cost, non- or low-concentrating solar-thermal collectors (50 °C to 150 °C). In this paper, an integrated computer-aided molecular and DAR (CAMD-DAR) system design framework is proposed that uses a group-contribution equation-of-state based on the statistical associating fluid theory (SAFT-γ Mie) for working-fluid design and property prediction simultaneously with the DAR module design. Following a detailed presentation of this CAMD-DAR system framework, the framework is employed to identify optimal organic working fluids and DAR-system designs simultaneously for a specified solar-cooling application. The results suggest that non-polar organic refrigerants with polar absorbents are to be selected if maximum cooling rates are required from an otherwise conventional DAR module design. In particular, a mixture of 2-butene (2-C_4H_8) and ethanol (C_2H_5OH) pressurised by He is identified as the optimum working fluid for a wide range of cooling and ambient temperatures. The use of this fluid can produce maximum cooling rates up to 146 W from 440 W of heat supplied to the generator at 82 °C, corresponding to a specific purchase cost (SPC) of £ 7.46 per W of cooling, and a coefficient of performance (COP) of 0.33 at a cooling temperature of 4 °C and an ambient of 20 °C. Overall, the proposed CAMD-DAR framework is capable of suggesting alternative organic working fluid mixtures that compete with the standard NH_3—H_2O pair, thanks to the lower generator temperatures (< 150 °C) required by these fluids to activate the DAR modules, which is especially advantageous in solar-cooling applications, when non- or low-concentrating collectors are to be used.

1. Introduction

Energy consumption for cooling purposes has been markedly increasing [1], whereby there is a growing interest in developing alternative sustainable cooling technologies. Notably, solar-driven cooling technologies in Africa show great potential to meet this escalating demand in cooling activities [2]. Diffusion absorption refrigeration (DAR), invented by Von Platen and Munters in the late 1920s [3,4], is a thermal-driven cooling technology that can be solar-driven, hence, can offer a great alternative to meet small-scale off-grid cooling demand [5].

A typical DAR module is shown in Fig. 1. DAR modules use three-component working fluids: refrigerant; absorbent; and auxiliary gas. A refrigerant-rich solution (State 1) is heated in the generator. In principle, the generated vapour (at State 2) forms a train of Taylor plugs that lifts the rich-solution slugs through a bubble-pump tube [6]. When using a volatile absorbent, a bubble pump is inefficient in desorbing all the refrigerant. Thus, a rectifier takes the vapour (State 4) and purifies it as partial condensation occurs. Stripped refrigerant-weak solution (State 5) mixes with the liquid separated at the bubble-pump top (State 3). This weak solution spills down the bubble pump outer

* Corresponding author.
E-mail address: c.markides@imperial.ac.uk (C.N. Markides).

https://doi.org/10.1016/j.enconman.2025.120067
Received 1 February 2025; Received in revised form 28 May 2025; Accepted 9 June 2025
Available online 23 July 2025
0196-8904/© 2025 The Authors. Published by Elsevier Ltd. This is an open access article under the CC BY license (http://creativecommons.org/licenses/by/4.0/).

Nomenclature

Acronyms

AAD	Average absolute deviation
AIT	Auto-ignition temperature
ASTM	American Society for Testing and Materials
CAMD	Computer-aided molecular design
CEPCI	Chemical engineering plant cost index
DAR	Diffusion absorption refrigeration
EoS	Equation of state
GC	Group contribution
GWP	Global warming potential
IAPWS	International Association of Pure Water and Steam
LB	Lower bound
LC	Lethal concentration
MINLP	Mixed-integer nonlinear programming
MP	Master problem
NLP	Nonlinear programming
NNC	Normalised normal constraint
NSGA	Non-dominated genetic algorithm
OAERAP	Outer approximation-equality relaxation-augmented penalty
ODP	Ozone depletion potential
ORC	Organic Rankine cycle
SAFT	Statistical associating fluid theory
SQP	Sequential quadratic programming
UB	Upper bound
VAT	Value-added tax
VLE	Vapour–liquid equilibrium

Variables

A	Helmholtz free energy
$\hat{c}_p$	Mass-specific constant-pressure heat capacity [$\mathrm{J\,kg^{-1}\,K^{-1}}$]
C	Cost
COP	Coefficient of performance
f	Function
$\hat{h}$	Mass-specific enthalpy [$\mathrm{J\,kg^{-1}}$]
k_B	Boltzmann's constant [$1.381 \times 10^{-23}\,\mathrm{J\,K^{-1}}$]
$\dot{m}$	Mass flowrate [$\mathrm{kg\,s^{-1}}$]
MW	Molecular weight [$\mathrm{kg\,mol^{-1}}$]
N	Number of molecules/groups
n	Group or site multiplicity in given molecular structure [mol]
p	Pressure [bar, Pa]
$\dot{Q}$	Heat transfer rate [W]
q''	Heat flux [$\mathrm{W\,m^{-2}\,K^{-1}}$]
SPC	Specific cooling cost [£ $\mathrm{W^{-1}}$]
T	Temperature [°C, K]
u	Linear velocity [$\mathrm{m\,s^{-1}}$]
V	DAR cooling unit volume [L]
$\tilde{x}$	Liquid-phase molar composition
x	Liquid-phase mass composition
y	Vapour-phase mass composition

Number sets

$\mathbb{R}$	Real number
$\mathbb{Z}$	Natural number

Greek symbols

β	Integer decision variable array
θ	Continuous decision variable array
Δ	Change
Γ	Flammability number
ρ	Mass density [$\mathrm{kg\,m^{-3}}$]

Subscripts and Superscripts

0	Initial
j	Compound index
k,l	Group indices
abs	Absorber
absr	Absorbent
an	Annular
b	Normal boiling point
bp	Bubble pump
bs	Bubble-to-slug transition
bub	Bubble point
c	Critical
calc	Calculated
ch	Charge
co	Cooling, or cold
cond	Condenser
CU	Cooling unit
dew	Dew point
evap	Evaporator
exp	Expansion
expt	Experimental
g	Auxiliary gas
gen	Generator
L	Liquid
max	Maximum
min	Minimum
mono	Monomer
rect	Rectifier
refr	Refrigerant
rs	Refrigerant-rich solution
sat	Saturation
V	Vapour
ws	Refrigerant-weak solution

tube to the absorber through a solution heat exchanger. The vapour refrigerant leaving the rectifier at State 6 is admitted to a finned air-cooled condenser and leaves as saturated or subcooled liquid (State 7). Sometimes, vapour (State 7′) may leave the condenser and bypass the evaporator.

Condensed refrigerant and auxiliary gas are subcooled in a gas heat exchanger. The subcooled streams (State 9′) mix adiabatically. According to Dalton's law, the adiabatic mixing is accompanied by refrigerant expansion due to the drop in temperature and refrigerant partial pressure (State 9) [6]. As the refrigerant-gas mixture flows down the evaporator tube, the refrigerant expands, removing heat from the gas heat exchanger and the cold space. The emerging mixture (State 10) leaves the evaporator, merging with any refrigerant bypass (State 7′) in the reservoir. The combined gas rises in the absorber and meets the pre-cooled weak solution (State 8), and almost all the refrigerant is absorbed. The auxiliary gas (State 8,g) leaves the absorber coil towards the gas heat exchanger. Meanwhile, the refrigerant-rich solution (State 11) flows to the solution heat exchanger. In the solution

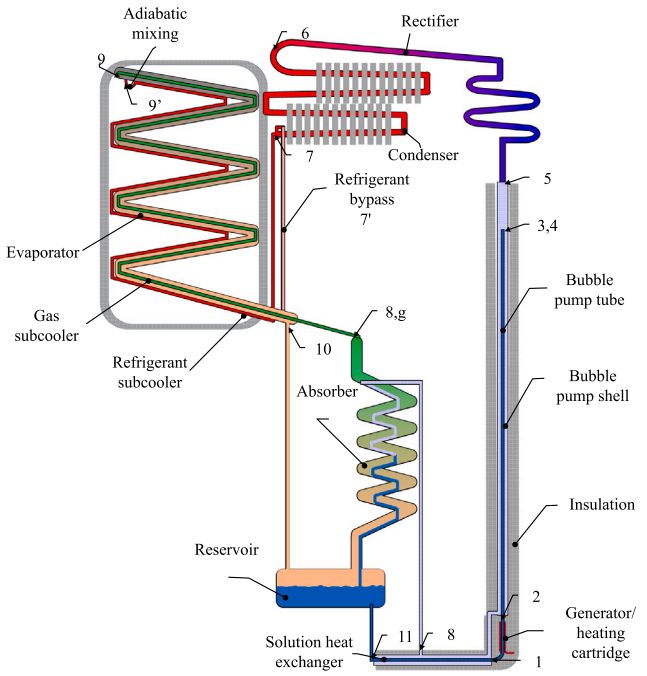

Fig. 1. Schematic diagram of a typical DAR module.

heat exchanger, the rich solution is preheated by the spilling-down weak solution before flowing into the generator again. The considered DAR shown in Fig. 1 is specified by having a semi-attached bubble-pump configuration as recommended by Zohar et al. [7] and tested by Kim et al. [8].

Commercial DAR modules commonly use ammonia—water (NH_3—H_2O) as the refrigerant–absorbent working-fluid pair and hydrogen or helium as the auxiliary gas [5,6,9]. The ammonia—water mixture is favoured due to its chemical stability within a large range of operating pressures and temperatures [6]. In addition, NH_3 offers a high latent heat of evaporation and a low freezing point (−77 °C) [10], allowing for more sub-zero cooling applications. This comes at the expense of the required generator temperatures to activate the bubble pump for NH_3—H_2O DAR modules, which can exceed 150 °C [11–15]. This high generation temperature challenges the effort paid to propose solar-powered DAR modules that can operate using low-cost non- or low-concentrating solar collectors which provide a heat source 50 °C to 150 °C [12,16–23].

Accordingly, bringing down the required temperature for generator activation has motivated investigating alternative working fluids [9, 24–27]. Many authors [8,17,28–40] discussed the potential use of organic working fluids such as butane—nonane (n-C_4H_{10}—n-C_9H_{20}) for DAR modules. Some of these working-fluid systems are reviewed by Rodríguez-Muñoz and Belman-Flore [5]. Amongst these efforts, there have been experiments demonstrating the validity of using organic-based working fluids to produce refrigeration using DAR modules [8, 38,39,41]. Some of these studies showed promising performance of organic-based DAR modules in comparison with NH_3—H_2O-based ones (*i.e.*, Ben Ezzine et al. [17]), though Zohar et al. [29] numerically demonstrated lower performance of DAR modules operating using some organic-based working fluids in favour of NH_3—H_2O DAR modules.

Following the discussion above, the general approach has been to investigate different working-fluid systems for operating DAR modules heuristically. Alternatively, a systematic approach using computer-aided molecular and DAR system design (CAMD-DAR) can advantageously integrate working-fluid design with DAR system optimisation over a range of operating conditions (*i.e.*, variable ambient conditions and variable heat available) [9,26,27,42]. Computer-aided molecular design (CAMD) involves the design of new molecules from their fragments under specified system design and/or operational limitations, and molecular feasibility constraints [43–45]. Integrating molecular and system designs ensures that more information about the system and molecular structure is well captured by incorporating the system model [46]. Either a screening methodology [47–49], or an optimisation method [50–60] is needed to design the pure-component molecule or mixture of interest.

CAMD has been applied for refrigerant selection [47–51,53,54,61, 62]. Nevertheless, limited literature is found on deploying systematic computer-aided molecular *and system* design in the context of designing alternative working fluids for absorption refrigeration systems using optimisation rather than screening [27]. Tora [54] considered refrigerant-absorbent pairs for such systems using a systematic, modular computer-aided molecular and system design approach. However, this did not include the system model while designing the working fluid, and thus, did not allow predicting mixture properties at actual operating conditions. Separating the selection of refrigerant and absorbent also overlooks molecular interactions between pairs, particularly at actual operating conditions, potentially excluding some pairs leading to sub-optimal solutions [57]. Papadopoulos et al. [60] proposed an integrated CAMD approach which can simultaneously design the refrigerant and absorbent, relying on absorption–refrigeration system performance rather than targeting physical properties, overcoming the limitations of earlier approaches. However, in the framework of Papadopoulos et al. [60], an empirical working-fluid thermodynamic model was adopted, and although very useful and reliable within certain (training) parameter ranges, such empirical models can perform less well outside these ranges [63].

In our current work we present a holistic CAMD-DAR framework modelled as an MINLP problem that can propose alternative organic-based working fluids for DAR operation using low-temperature heat sources like non- or low-concentrating solar-thermal collectors. In Section 2, the developed CAMD-DAR framework is presented with a special interest in describing the DAR thermodynamic model (Section 2.1), including how the DAR module is sized and costed for the thermoeconomic evaluations (Section 2.2). The CAMD-DAR framework is formulated as an MINLP optimisation problem in Section 2.3 defining two case studies. The employed optimisation methods are listed in Section 2.4. Different CAMD-DAR model components are valid according to the strategy presented in Section 2.5. The CAMD-DAR results are presented and discussed in Section 3. Firstly, the CAMD-DAR results for the first case study considering only simple non-polar hydrocarbons presented in Section 3.1, and CAMD-DAR results for the second case study considering polar and non-polar hydrocarbons are presented in Section 3.2. In Section 3.3 the importance of the compromise between cooling rate and cost is emphasised, by showing the results of multi-objective optimisation. Finally, the paper closes with some key concluding remarks in Section 4.

2. Methodology and DAR-CAMD problem definition

The CAMD-DAR framework structure shown in Fig. 2 integrates the design of a working-fluid mixture: refrigerant; absorbent; and auxiliary gas, with the optimisation of other DAR operating conditions such as charging pressure; refrigerant-rich solution charging composition and module size. The CAMD-DAR framework is built up of five main components: a DAR system model; a working-fluid model based on the SAFT-γ Mie GC-EoS [64]; a costing method; system and molecular constraints; and finally, the optimisation methods used in this paper.

2.1. DAR thermodynamic model using SAFT-γ Mie

For the integrated CAMD-DAR framework, a DAR thermodynamic model is needed. Many authors have modelled DAR systems [7,11, 29,32,65,65–73]. Unlike other authors, who mostly use empirical EoS

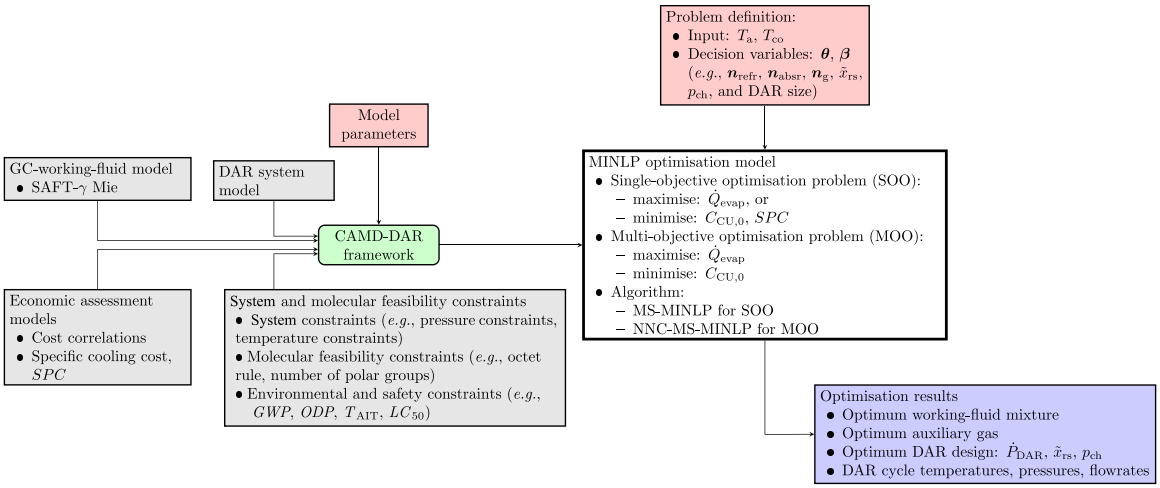

Fig. 2. Proposed integrated computer-aided molecular and DAR-system design (CAMD-DAR) framework.

(mainly Pátek and Klomfar [74] to model the NH_3—H_2O mixture), Harraz et al. [26,42] introduced the use of the GC SAFT-γ Mie [64] EoS in their DAR modelling framework. With a few exceptions, previous models in the literature are limited to those for which pre-selected working fluids are considered for thermodynamic and thermoeconomic assessment of DAR modules. To ensure transferability to different DAR systems and working fluids, a fundamental thermodynamic model for the DAR cycle, based on energy and mass conservation, is adopted based on the conservation of energy and mass, avoiding – whenever possible – the use of system-specific correlations. The presented model is detailed in an appendix, in Table A.1.

In our current work, group-contribution (GC) methods, wherein molecules are modelled as a set of fragments, are considered. Molecular groups are defined (*i.e.*, –CH_3, >CH_2, >CH–, >C<, …, *etc.*), and each contributes proportionally according to some indicator. This approach has been extended to consider mixtures in addition to pure components to predict thermodynamic and thermophysical properties [75]. GC methods are straightforward and tractable, making them user-friendly within an acceptable margin of accuracy. A GC equation-of-state (EoS) is needed to predict the thermodynamic properties of pure components and mixtures and evaluate phase equilibria as required. Early GC approaches include the implementation of the Joback and Reid GC method [76] and the UNIFAC model [77–79], and its variants. These methods are empirical; hence, they perform well only within the training range and, in the case of activity-coefficient models like UNIFAC, target liquid-phase (rather than vapour-phase) properties [63]. Alternatively, molecular-based equations of states such as those based on statistical associating fluid theory (SAFT) [80,81] ensure reliable predictions of a wider variety of thermodynamic properties across broader ranges of temperatures and pressures.

SAFT is a molecular-based theory with a firm foundation in statistical mechanics. The incorporation of the thermodynamic perturbation theory (TPT1) of Wertheim [82–85] allows the accounting not only of molecular shape but, crucially in our present study, intermolecular association (such as hydrogen bonding) that is often a feature of polar molecules that would be attractive for DAR. Moreover, its molecular basis makes SAFT predictive; it can be used for reliable predictions of a wider variety of thermodynamic properties across broader ranges of temperatures and pressures than traditional cubic EoS. In our current work thermodynamic properties are evaluated using the GC equation of state, SAFTγ Mie [64,86–88].

SAFT-γ Mie has been described in detail elsewhere [64] and summarised extensively in a comprehensive review [88] of SAFT-γ Mie modelling. Only a brief summary is provided here. Molecules are modelled as chains of molecular-group segments that can associate. The Helmholtz free energy, A of the fluid is broken down into contributions according to:

$$\frac{A}{N\mathrm{k_B}T} = \frac{A^{\mathrm{ideal}}}{N\mathrm{k_B}T} + \frac{A^{\mathrm{mono}}}{N\mathrm{k_B}T} + \frac{A^{\mathrm{chain}}}{N\mathrm{k_B}T} + \frac{A^{\mathrm{assoc}}}{N\mathrm{k_B}T}\,, \tag{1}$$

where N refers to the number of molecules in the system, $\mathrm{k_B}$ is the Boltzmann constant, and T refers to the system absolute temperature. Here, A^{ideal} is the ideal (or kinetic) contribution; A^{mono} is the monomer contribution (comprising dispersive and repulsive interactions of the fluid of monomeric segments); A^{chain} is the contribution due to chain formation (the aggregation of the monomeric segments); and A^{assoc} is the contribution due to the intermolecular association (whenever association sites are present, *e.g.*, to represent hydrogen bonding). The interaction between two segments is described using a Mie (generalised Lennard-Jones) potential [64,88].

In our current work, nine organic functional groups in addition to ammonia and water are considered: H_2O; NH_3; –CH_3; >CH_2; >CH–; =CH_2; =CH–; –CH_2OH; –OH; –NH_2; and >NH. For the considered groups, like-group parameters, unlike-group parameters and unlike-group association parameters are taken from the literature [64,86,88–91]. To accurately model any associating working pair, cross-interaction parameters are required. Without explicit values for unlike-group cross-interaction parameters, the unlike-group diameter is estimated [86,92] using the Lorentz arithmetic-mean combining rule, and the dispersion energy between unlike groups is estimated using an augmented geometric-mean rule [86,88]. The ideal-gas contributions to the heat capacity, enthalpy of formation and entropy of formation are evaluated using the correlations of Joback and Reid [76].

Methods from the literature are adopted to estimate surface tension for variable-structure molecular compounds. In the case of the ammonia—water mixture, these are predicted as suggested in Ref. [93] assuming a quasi-ideal mixture. For other organic compounds, either the method of Sugden [94] (for non-polar organic compounds) or the Sastri and Rao [95] method (for polar organic compounds) is adopted. The IAPWS method [96] is used for calculating pure-component surface tensions of water, and ideal-mixing rules are adopted to estimate the surface tension of organic mixtures. Any thermodynamic property (*e.g.*, ρ, T_b) needed for a surface-tension calculation is evaluated using SAFT-γ Mie, while critical properties for organic compounds are calculated using GC methods developed by Joback and Reid [76].

The DAR-model inputs presented in Eqs. (2a) to (2i) in Table 1 are considered. Eq. (2a) assumes the generation step starts with a saturated-liquid refrigerant-rich working-fluid mixture [11,65,97]. Due to difficulty measuring flow temperatures, DAR temperature measurements are taken at the walls. For an operating DAR module, the heat-transfer rate is sufficiently high that the working-fluid temperature

Table 1
DAR system model inputs for considered thermoeconomic optimisation and analysis.

Description	DAR model input	
Generator inlet temperature	$T_1 = T_{bub}\left(p_{ch}, x_{rs}\right)$	(2a)
Generator outlet temperature	$\Delta T_{gen,o} = T_{gen,w} - T_2 = \Delta T_{lo}$	(2b)
Bubble-pump outlet temperature	$T_3 = T_4 = T_2 - 2$	(2c)
Rectifier liquid temperature	$T_5 = T_3 - 5$	(2d)
Rectifier vapour temperature	$T_6 = T_{sat,refr}\left(p_{ch}\right)$	(2e)
Condenser outlet temperature	$\Delta T_{cond,o} = T_7 - T_a = \Delta T_{lo}$	(2f)
Desorbed gas temperature	$T_{8,g} = T_a + 0.1$	(2g)
Expansion temperature drop	$\Delta T_{exp} = T_{9'} - T_9 = (18.5 - 0.15 \times p_{ch})$	(2h)
Reservoir temperature	$T_{11} = T_7$	(2i)

in the generator is reasonably assumed to approach the generator wall temperature as represented by Eq. (2b) [12,98]. Following the model proposed by Zohar et al. [7,11], the temperature drops across the bubble pump and between rectifier liquid and vapour at the top of the bubble pump are assumed to be 2 °C and 5 °C, respectively as demonstrated by Eqs. (2c) and (2d).

For most organic pairs presented later, the bubble-pump vapour effluent has higher purity compared to ammonia—water mixtures at similar operating conditions. In addition, it is reasonable to design DAR module charge pressure to ensure recovery of pure refrigerant, thus considering Eq. (2e). Moreover, complete condensation should be sought in DAR design, such that subcooled refrigerant leaves the condenser approaching ambient temperature, which is considered by Eq. (2f), ensuring that the DAR design has a large enough condenser. The auxiliary gas escaping the absorber also is assumed to approach ambient temperature as described by Eq. (2g) [98]. In contrast, the temperature difference across the gas-refrigerant mixing step is described by Eq. (2h) developed by Freeman [98]. Finally, for simplicity, many authors (see Refs. [6,11,65]) consider refrigerant-rich working fluid mixture leaves the absorber as temperate as the condenser effluent as presented by Eq. (2i).

2.2. DAR module sizing and costing based on commercial data

Estimating the DAR purchased cost is crucial in performing the thermoeconomic assessment of DAR modules. One approach is to deal with the DAR module cost in terms of the costs of its components, similar to what is conventionally done with other heat pumps [56,58]. However, it has been found challenging to use correlations from literature to size heat-exchange areas for a given DAR module (*e.g.*, condenser, absorber, evaporator). Most heat-exchanger sizing and costing correlations available in the literature (see Refs. [45,99]) are not intended to fit small-component sizes that are encountered in small-scale DAR modules and can hardly be validated, especially in the absence of detailed heat and mass transfer measurements for DAR modules. It is also noticed that DAR cooling modules are sold and replaced as a single welded module, unlike conventional vapour-compression refrigeration systems. In other words, an end-user cannot replace just one of the DAR components. Available DAR modules in the market are rated using their cooling volume capacity (V_{CU}) and their supplied heat rate ($\dot{Q}_{gen}$) [100]. As seen in Fig. 3(a), there is a direct correlation between the cooling-unit volume capacity (in litres) and the supplied heat rate (in W), such that:

$$\dot{Q}_{gen} = 1.55 V_{CU}. \tag{3}$$

Following the discussion above, finding a costing method that can relate DAR design parameters to price is tractable. The market for DAR has relatively expanded with time; DAR modules of 28 L capacity (perfect for camping) up to 520 L capacity (suitable for households) are sold. Small-capacity DAR modules can operate using as low as 50 W supplied heat rate, while larger capacity units are rated to operate with 500 W.

It can be noticed in Fig. 3(b) that for the same DAR supplied heat rate, $\dot{Q}_{gen}$, there is a large variation in the purchase price, which can be partially due to model differences or provision by different manufacturers. To correlate the DAR module purchase price to $\dot{Q}_{gen}$, 237 data points were gathered from six suppliers for seven cooling-unit manufacturers for four fridge makes. Prices, collected from suppliers' websites in the American and British markets, were corrected for inflation using the Chemical Engineering Plant Cost Indices (CEPCI) for 2019 and 2022, which take values of 607.5 and 816.3, respectively [102]. Prices in US$ were converted to GB£ using 2022-average exchange rate of £1 = $1.2054 [101]. Nonlinear regression was performed, yeilding

$$C_{CU,0} = 32\dot{Q}_{gen}^{0.58}, \tag{4}$$

where $C_{CU,0}$ is the installed cost (including shipping expenses and VAT) of a DAR module rated with supplied heat rate. The fitted parameters were estimated using a Levenberg–Marquardt algorithm [103,104] to minimise the difference between the market and calculated prices. Eq. (4), which is plotted in Fig. 3(b), reproduces DAR purchase cost with percent absolute average deviation, % AAD of 18%. It should be stressed that this relatively high AAD is attributed to the aforementioned large variation in some market data; it was chosen not to exclude any of these prices to reflect the wide variation of the market as it is still relatively niche compared to other more-stable technologies, which may suffer fewer price variations.

2.3. CAMD-DAR problem definition

As mentioned earlier, the goal of this paper is to present a CAMD-DAR framework to design working fluids for running DAR using non- or low-concentrating solar-thermal collectors compared to ammonia—water systems. The following organic functional groups are considered for both refrigerant and absorbent design: $-CH_3$, $>CH_2$, >CH–, $=CH_2$, =CH–, $-CH_2OH$, –OH, $-NH_2$ and >NH, which can form compounds that belong to one of the families listed in Table 2, while hydrogen and helium are considered alternatives for the choice of the auxiliary gas. This functional-group list is selected to represent low-GWP organic compounds and some polar organic compounds, such as those relevant to ammonia (*e.g.*, amines). Although out of the scope of this paper, it is worth mentioning that this list can be extended to use other organic functional groups subject to the availability of relevant thermodynamic models.

The optimisation problem considered in this paper can be defined as:

$$\begin{aligned} \max_{\substack{\tilde{x}_{rs}, p_{ch}, \bar{p}_9, \dot{Q}_{gen}, \\ \boldsymbol{n}_{refr}, \boldsymbol{n}_{absr}, \boldsymbol{n}_g}} \quad & f\left\{\tilde{x}_{rs}, p_{ch}, \bar{p}_9, \dot{Q}_{gen}, \boldsymbol{n}_{refr}, \boldsymbol{n}_{absr}, \boldsymbol{n}_g\right\} \\ \text{s.t.} \quad & \boldsymbol{h}(\boldsymbol{\theta}, \boldsymbol{\beta}) = 0, \\ & \boldsymbol{g}(\boldsymbol{\theta}, \boldsymbol{\beta}) \le 0, \\ & \boldsymbol{\theta} \in \left[\boldsymbol{\theta}^{LB}, \boldsymbol{\theta}^{UB}\right] \subseteq \mathbb{R}^n, \\ & \boldsymbol{\beta} \in \left[\boldsymbol{\beta}^{LB}, \boldsymbol{\beta}^{UB}\right] \subseteq \mathbb{Z}^m. \end{aligned} \tag{5}$$

where $\boldsymbol{\theta}$ is the set of continuous decision variables (*e.g.*, p_{ch}, $\tilde{x}_{ch}$), $\boldsymbol{\beta}$ is the set of integer decision variables (*e.g.*, $\boldsymbol{n}_{refr}$, $\boldsymbol{n}_{abs}$, $\boldsymbol{n}_g$), and f is

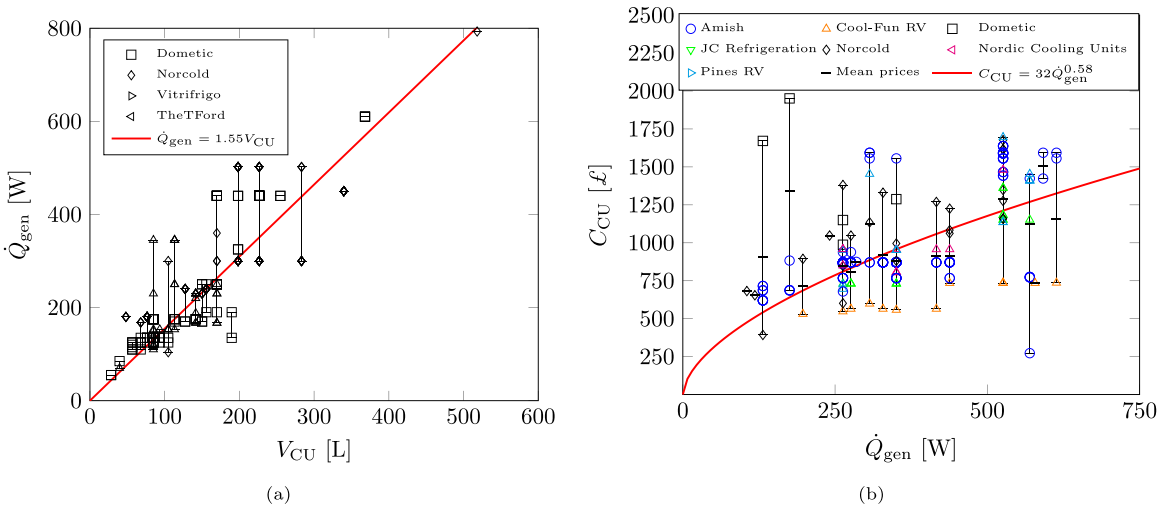

Fig. 3. DAR cost data and models for the present CAMD-DAR framework. (a) DAR supplied heat rate. (b) Purchase prices of commercial DAR cooling units. All prices are presented in GB£; prices available in US$ are converted to £ using the 2022-average exchange rate of £ 1 = $ 1.2054 [101].

Table 2
Organic families, their structural formulae and constituent functional groups as considered in this study, where n represents the number of CH_2 groups in corresponding molecules. – denotes one single bond, > denotes two single bonds and = denotes one double bond.

Hydrocarbon family	Structural forumla	Functional groups
n-alkanes (n-C_nH_{2n+2})	CH_3–$[CH_2]_n$–CH_3	–CH_3 and >CH_2
2-alkanes (2-C_nH_{2n+2})	$[CH_3]_2$>CH–$[CH_2]_n$–CH_3	–CH_3, >CH_2 and >CH–
n-alkenes (1-C_nH_{2n})	CH_2=CH–$[CH_2]_n$–CH_3	–CH_3, >CH_2, =CH_2 and =CH–
2-alkenes (2-C_nH_{2n})	CH_3–CH=CH–$[CH_2]_n$–CH_3	–CH_3, >CH_2 and =CH–
1-amines (1-$C_nH_{2n+1}NH_2$)	CH_3–$[CH_2]_n$–NH_2	–CH_3, >CH_2 and –NH_2
2-amines (2-$C_nH_{2n+1}NH_2$)	$[CH_3]_2$>CH–$[CH_2]_n$–NH_2	–CH_3, >CH_2 >CH– and –NH_2
2°-amines (2°-$C_nH_{2n+2}NH$)	$[CH_3]_2$>NH–$[CH_2]_n$–CH_3	–CH_3, >CH_2 and >NH
1-alcohols (1-$C_nH_{2n+1}OH$)	CH_3–$[CH_2]_n$–OH	–CH_3, >CH_2 and –OH/–CH_2OH

the objective function, which can be, for instance, $-\dot{Q}_{evap}$ or $C_{CU,0}$. The vectors of $\boldsymbol{h}(\boldsymbol{\theta},\boldsymbol{\beta})= 0$, and $\boldsymbol{g}(\boldsymbol{\theta},\boldsymbol{\beta})\leq 0$, respectively, represent the sets of equality and inequality constraints relevant to DAR, which are listed in Table 3. The vectors $\boldsymbol{\theta}^{LB}$, $\boldsymbol{\theta}^{UB}$, $\boldsymbol{\beta}^{LB}$, $\boldsymbol{\beta}^{UB}$ are lower and upper bounds imposed on the continuous and integer decision variables, which are listed in Tables 3 and 4, respectively. In the present work, various optimisation objectives are sought. It is common to consider maximising the cooling rate, $\dot{Q}_{evap}$ as an objective function. Considering the thermoeconomic evaluation of DAR for distributed refrigeration, two other objective functions are considered: minimising the total DAR fridge cost, $C_{CU,0}$ and minimising SPC:

$$SPC = C_{CU,0}/\dot{Q}_{evap}. \tag{6}$$

To ensure the feasibility of proposed DAR designs, various constraints summarised in Table 3 are considered to complement the presented framework. These constraints are grouped into three classes: system constraints (Eqs. (7) to (11)); molecular-feasibility constraints (Eqs. (15) to (17)); and environmental and safety constraints (Eqs. (19) to (21)).

Eqs. (7a) and (7c) are employed to ensure that for a proposed working fluid, the two-phase mixture generated has enough slugs to push the working fluid up the bubble pump, where u_L and u_v are, respectively, the superficial velocities of coexisting liquid and vapour phases. The bubble-to-slug transition velocity, $u_{L,bs}$ and the slug-to-annular transition velocity, $u_{V,an}$, are calculated using the model set by Taitel et al. [105].

Eq. (8a) indicates partial refrigerant pressure at the beginning of evaporation should be suppressed by its partial pressure at the end of the evaporation step to ensure feasible cooling; p_9 is refrigerant partial pressure after adiabatic mixing (at evaporator inlet, State 9), and p_{10} is the refrigerant partial pressure at the evaporator outlet (State 10). Eqs. (8b) and (8c) impose constraints on the evaporator lowest pressure to ensure cooling. The constraints in Eqs. (8e) (8f) impose limitations on DAR charging pressure, which should not exceed an allowable maximum pressure, $p_{max} = \min\left(21\ \text{bar}, 0.85 \cdot p_{c,min}\right)$. To ensure that the DAR module operates above ambient pressure and allows complete refrigerant condensation, the charge pressure should be greater than or equal a minimum charging pressure, $p_{min} = \max\left(2\ \text{bar}, p_{sat,1}\left(T_a + 5\right)\right)$.

Eq. (9a) ensures a positive temperature gradient across the rectifier, while Eq. (9b) limits DAR operation to when generator wall temperature suppresses refrigerant-rich solution bubble temperature. This limitation ensures robust calculation for the generator. The constraint represented by Eq. (9c) imposes a check that refrigerant is more volatile than absorbent at DAR system pressure.

The constraint in Eq. (10a) ensures the refrigerant-weak solution composition is lower than that of the refrigerant-rich solution to ensure a positive composition gradient across the absorber, while the constraint in Eq. (10b) limits the weak-solution composition to be lower than 10 mol %. Weak-solution compositions below 10 mol % ensure a thermodynamically favoured absorption.

The constraint in Eq. (11) ensures a positive net $\dot{Q}_{evap}$ in the evaporator, where $\dot{Q}_{evap,refr}$ is the net enthalpy difference for the refrigerant across the evaporator and $\dot{Q}_{evap,g}$ is the net enthalpy difference for the auxiliary across the evaporator. This constraint is intended to prevent the optimiser from ending with some working-fluid mixtures, which at operating conditions result in a negative net $\dot{Q}_{evap}$.

To ensure that the formed molecules are chemically feasible, additional molecular feasibility constraints are needed, such as those proposed by Odele and Macchietto [106], and Churi and Achenie [51]. For a given component, j in the working-fluid mixture, available bonds, $v_{k,j}$ of functional group, k must suffice eight electrons in the outermost electron shell of the central atoms (C, N, O) in the functional groups of

Table 3
List of constraints involved in the CAMD-DAR framework representing the set of equality constraints, $\boldsymbol{h}(\boldsymbol{\theta},\boldsymbol{\beta})=0$ and set inequality constraints, $\boldsymbol{g}(\boldsymbol{\theta},\boldsymbol{\beta})\leq 0$, which are relevant to the DAR system. The constraints are classified as system-related constraints, molecular-feasibility-related constraints or safety-and-environmental-related constraints.

System constraints		
- Bubble pump		
$d_{bp}=0.05$	(limitation on the bubble-pump tube diameter [m])	(7a)
$u_L \leq u_{L,bs}$	(No bubbly flow)	(7b)
$u_{V,an} \leq u_V$	(No annular flow)	(7c)
- Pressure constraints		
$p_9 \leq p_{10}$	(Evaporator pressure build up)	(8a)
$0.02 \leq p_9$	(Lower bound for Evaporator-pressure build up)	(8b)
$p_9 \leq 0.2$	(Upper bound for Evaporator-pressure build up)	(8c)
$p_{10} \leq p_{evap,max}$	(Evaporator maximum pressure)	(8d)
$p_{ch} \leq \min\left(25\ \text{bar}, 0.85 p_{c,min}\right)$ bar	(Feasible charge pressure 1)	(8e)
$\max\left(2\ \text{bar}, p_{sat,1}\left(T_a+5\right)\right) \leq p_{ch}$	(Feasible charge pressure 2)	(8f)
- Temperature constraints		
$T_{sat,refr} < T_{bub,rs}$	(Temperature gradient across the rectifier)	(9a)
$T_{bub,rs} < T_{gen,w}$	(Driving force at generator wall)	(9b)
$T_{sat,refr} < T_{sat,absr}$	(Working-fluid relative volatility)	(9c)
- Composition constraints		
$\tilde{x}_{ws} < \tilde{x}_{rs}$	(Feasible absorption)	(10a)
$\tilde{x}_{ws} < \tilde{x}_{ws,min}$	(High absorption affinity)	(10b)
$0.1 \leq \tilde{x}_{rs}$	(Lower bound for rich-solution composition)	(10c)
$\tilde{x}_{rs} \leq 0.38$	(Upper bound for rich-solution composition)	(10d)
- Heat flow		
$\dot{Q}_{evap,g} < \dot{Q}_{evap,refr}$	(Positive cooling capacity)	(11)
$50 \leq \dot{Q}_{gen}$	(Lower bound for generator heat rate)	(12)
$\dot{Q}_{gen} \leq 500$	(Upper bound for generator heat rate)	(13)
Molecular feasibility constraints		
- Lower and Upper Bounds		
$n_{k,j}^{LB} \leq n_{k,j}$	$\forall j \in [\text{refr}, \text{absr}]$ & $\forall k = 1 : N_G$	(14a)
$n_{k,j} \leq n_{k,j}^{UB}$	Values for $n_{k,j}^{LB}$ & $n_{k,j}^{UB}$ are listed in Table 4	(14b)
- Octet rule		
$2m_j = \sum_{k=1}^{N_{G,j}} (2-v_k)\, n_{k,j}$	$\forall j \in [\text{refr}, \text{absr}]$	(15)
- Olefin		
$0 \leq \cos\left[\pi\left(n_{=CH_2,j} + n_{=CH-,j}\right)\right]$		(16a)
$n_{=CH_2,j} \leq n_{=CH-,j}$		(16b)
- Polar groups		
$n_{-NH_2,j} + n_{-CH_2OH,j} + n_{>NH,j} + n_{-OH,j} = 1$		(17)
- Auxiliary gas		
$n_{H_2,j} + n_{He,j} = 1$		(18)
Safety and environmental constraints		
- Safe operation		
$T_{gen,w} + 30 \leq T_{AIT,j}$	(Auto-ignition temperature)	(19a)
$\Gamma_j \leq 0.8$	(Flammability)	(19b)
- Environmental		
$\log_{10}(GWP_j) \leq \log_{10}(150)$	(Global warming potential)	(20a)
$\log_{10}(ODP_j) \leq \log_{10}(0.2)$	(Ozone depletion potential)	(20b)
- Health		
$1 < \log_{10}(LC_{50,j})$	(Toxicity)	(21)

* Further details of the implementation of safety and environmental constraints are provided in a Supplementary Material file.

Table 4
Upper and lower bounds for integer decision variables that represent molecular multiplicities considered in the CAMD-DAR framework.

j	Bound	$n_{-CH_3,j}$	$n_{>CH_2,j}$	$n_{=CH_2,j}$	$n_{=CH-,j}$	$n_{>CH-,j}$	$n_{-OH,j}$	$n_{-CH_2OH,j}$	$n_{-NH_2,j}$	$n_{>NH,j}$
"refr"	Lower	0	0	0	0	0	0	0	0	0
	Upper	2	5	1	2	1	1	1	1	1
"absr"	Lower	0	0	0	0	0	0	0	0	0
	Upper	2	9	1	2	1	1	1	1	1

interest. The well-known "octet rule" [106] stated in Eq. (15) ensures the chemical feasibility of designed working-fluid pair components, where $n_{k,j}$ is the number of occurrences of functional group, k in molecule, j. Only acyclic molecules for both refrigerant and absorbent are considered in this study, $m_j = 1$.

Two other constraints in Eq. (16) are important to ensure a feasible olefin compound is designed and to avoid mixing single and double bonds. The number of double-bond groups (*i.e.*, $=CH_2$ and $=CH-$) should be even as indicated in Eq. (16a), and the number of occurrences of the terminal group ($=CH_2$) should be less than or equal that of the internal group ($=CH-$) as constrained by Eq. (16b) [58,59].

To provide a compromise the between the robustness and reliability of the presented CAMD-DAR framework, molecules containing multiple polar groups are excluded, thereby obviating the need to consider second-order interaction effects within a given molecule and ensuring an accurate representation of the adopted thermodynamic models. Thus, the number of polar groups (*i.e.*, $-NH_2$, $-NH$, $-CH_2OH$, $-OH$) in a given molecule, j is constrained to only one, as described by Eq. (17). Only a single auxiliary gas is to be selected, which is imposed by Eq. (18).

It is crucial to ensure that the selected working-fluid pair alongside its substances (refrigerant and absorbent) comply with environmental and safety regulations. Consideration of environmental properties, such as *ODP*, *GWP*, flammability and toxicity in relation to CAMD of working fluids, including working-fluid mixtures, has been discussed in a recent review article [107] focusing on organic Rankine cycles (see, *e.g.*,

Sections 3.2, 4.8 and 7.1 therein); the discussion is equally pertinent in the context of DAR systems. In our current work, the constraint in Eq. (19a) implies that the highest temperature in the DAR module must be lower than the auto-ignition temperatures, $T_{AIT,j}$ of both the refrigerant and absorbent, eliminating any risk of ignition at an incidence of leakage to the atmosphere during operation [56,108]. The ASTM standard test method E659-78 defines the auto-ignition temperature, T_{AIT} as the lowest temperature at which a substance will ignite with a hot flame when it comes in contact with air at atmospheric pressure, without the aid of any external energy source such as a spark or flame. It is one of the essential safety specifications used to quantify the hazardous nature of a chemical substance. The absolute auto-ignition temperatures for pure substances are estimated using the GC method of Albahri et al. [109].

The constraint in Eq. (19b) ensures that the flammability (Γ-) numbers of the selected refrigerants and absorbents are at most 0.8 as recommended by Schilling et al. [56], to ensure that the working-fluid pair is not hazardously flammable. The method proposed by Kondo et al. [110] is adopted to predict the Γ-numbers for pure refrigerants and absorbents.

Eqs. (20a) and (20b) ensure the design of an environment-friendly refrigerant–absorbent pair; the global warming potential, *GWP* is estimated using the first-order GC method adopted from work by Hukkerikar et al. [111]. Recognising the risk of leakage or disposal in water, Eq. (21) is implemented to ensure the design of a low-toxicity working fluid. One way to express toxicity is the fathead minnow 96-h lethal concentration, LC_{50}(FM) endpoint, which represents the concentration in water which kills half of the fathead minnow (Pimephales promelas) in 4 days (96 h) [111]. For less-toxic working-fluid pairs, 96-h LC_{50} should be greater than or equal 10 $mg\,L^{-1}$ [56]. The LC_{50}(FM) can be estimated using the first-order GC method proposed by Hukkerikar et al. [111].

The MINLP CAMD-DAR framework is used to maximise cooling rate output over a range of ambient and cooling conditions: $10\,°C \leq T_a \leq 40\,°C$ and $-16\,°C \leq T_{co} = 8\,°C$. Two auxiliary gases are considered: hydrogen (H_2) and helium (He). Two case studies are considered in this paper, which are described below.

In the first case study, straight-chain non-polar working-fluid mixtures are considered. Thus, the following groups are varied for both absorbent and refrigerant: $–CH_3$; $>CH_2$; $=CH_2$; and =CH–. As polar groups are not considered in this MINLP, the constraints in Eq. (17) are redundant. The decision-variable space consists of four continuous and ten integer decision variables.

To allow for branched and polar working-fluid mixtures, in the second case study five additional groups (>CH–, –OH, $–CH_2OH$, $–NH_2$, and >NH) are considered for each of the refrigerant and absorbent. The system size is fixed, to mimic purchasing a commercial DAR module (*e.g.* [112,113]), and replacing the conventional working fluid (NH_3—H_2O—H_2) with new organic and environment-friendly working fluid. Further, varying the objective function is also considered to investigate the effect on the proposed working fluid and charging conditions. Three objective functions are considered: maximising the cooling, $\dot{Q}_{gen}$; minimising the purchase cost, $C_{CU,0}$; and minimising the specific purchase cost of cooling, SPC.

To extend the above discussion, multi-objective optimisation (MOO) is applied to offer a set of alternative designs that take into account the compromise between cooling rate and cost. The developed CAMD-DAR framework is used and an MINLP problem is formulated considering two simultaneous objective functions: minimising $C_{CU,0}$ and minimising $-\dot{Q}_{evap}$ (*i.e.*, maximising $\dot{Q}_{evap}$).

After solving the multi-objective optimisation, a Pareto front (the set of all non-dominated solutions [114]) is constructed. Being a non-dominated optimal solution means that there is no other better solution in one of the objectives' values without worsening the other objectives. It is important to ensure the generation of evenly-distributed non-dominated points to generate the Pareto front [115,116]. It is common to use scalarisation methods, such as weighted sum, in CAMD problems; however, these methods may not be able to generate an evenly-distributed set of solutions on the Pareto front. On the other hand, van Kleef et al. [58] applied a non-dominated sorting genetic algorithm (NSGA) to consider the thermodynamic and economic performance of organic Rankine cycles (ORCs) by designing working fluids. Lee et al. [115] reviewed different MINLP MOO approaches for the CAMD problem, where they presented trade-offs between different MOO algorithms in terms of convergence and computational time.

In our study, the normalised normal constraint (NNC) algorithm developed by Messac et al. [116] is used to formulate the MOO problem into a single-objective-function problem. The NNC method ensures a nice evenly spaced set of non-dominated optimal solutions. In addition, the NNC algorithm allows handling of two or more multi-objective functions. The formulated single-objective problem is solved using the hybrid optimisation algorithm, where all the obtained local and global optimum solutions are passed to a dominance filter proposed by Messac et al. [116] to generate the optimal Pareto front with non-dominated optimal solutions.

2.4. Optimisation algorithms

The CAMD-DAR framework implies a mixed-integer nonlinear optimisation problem. If the working-fluid mixture is predefined, the MINLP problem reduces to an NLP requiring optimisation of only continuous decision variables listed in Table 3. In our study, the hybrid stochastic-deterministic method implemented in gPROMS [117] for solving global optimisation problems is adopted to combine the advantages of both stochastic and deterministic approaches. The hybrid stochastic-deterministic approach avoids the limitation of how a single initial guess may affect the quality of the optimal solution. In addition, it allows more exploration of the decision-variable space.

The hybrid optimisation algorithm deployed in the present work uses a stochastic multi-start optimisation method. The algorithm is initialised by solving the MINLP problem using a user-defined initial guess ($\boldsymbol{\theta}^{(0)}$ and $\boldsymbol{\beta}^{(0)}$). Each MINLP is solved using an outer-approximation equation-relaxation augmented-penalty (OAERAP), a gradient-based optimisation algorithm specified at the next level of the hybrid optimisation method. Then, provided the number of initial guesses (which is specified by the user) is not exceeded, the optimiser generates a new unique random initial guess ($\boldsymbol{\theta}_i^{(0)}$ and $\boldsymbol{\beta}_i^{(0)}$). The solver uses the quasi-random Sobol [118] number generator to generate the initial guesses from a randomly distributed decision-variable space between its lower and upper bounds to provide an even distribution of unique sample points. The generated local optima are ranked, and this ranking is continuously updated.

In the present study, optimal alternatives that are similar (within 1%) are considered as a single optimal point. The number of initial guesses is set to 500, a value tuned to ensure that the best optimum point is achieved at least twice during each optimisation run, provided that the initial guesses are unique. At each iteration of the multi-start optimisation algorithm, the gradient-based OAERAP algorithm described by Viswanathan and Grossmann [119] is deployed to find the local optima for MINLP problems; the sequential quadratic program (SQP) [114] is used to solve the fully-relaxed and primal NLP problems to be addressed within each OAERAP optimisation. The implemented mixed-integer linear programming (MILP) solver is based on the revised simplex and Branch-and-Bound methods developed by Berkelaar et al. [120].

2.5. Model validation

The CAMD-DAR framework components depicted in Fig. 2 are validated, before running the CAMD MINLP optimisation problem. First, the DAR thermodynamic model is validated against experimental data. Then, the optimisation algorithm is validated to ensure convergence to global optima.

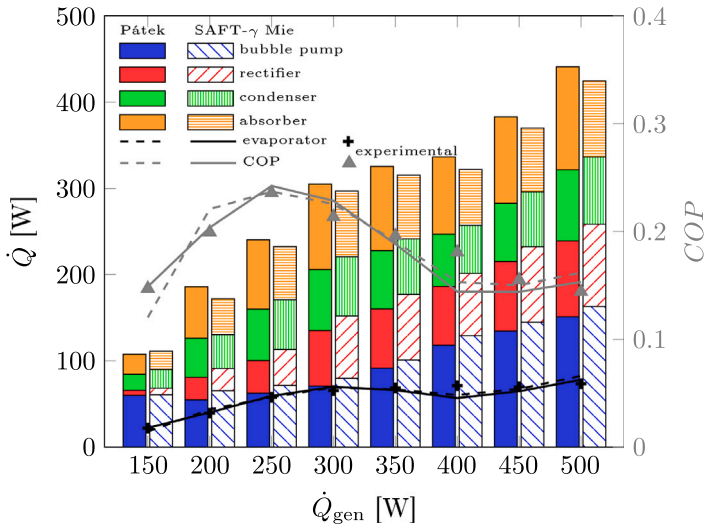

Fig. 4. Comparison between the proposed model using the SAFT-γ Mie EoS and that of Starace and De Pascalis [65] using Pátek and Klomfar equations [74], for $150 \leq \dot{Q}_{gen} \leq 500$, all compared against experimental data for an NH_3—H_2O—H_2 DAR module operating at p_{ch} = 17 bar and T_{co} = 5 °C.

2.5.1. DAR thermodynamic model

The presented DAR thermodynamic model is a modification of that of Starace and De Pascalis [65] however, whereas these authors used the empirical correlations of Pátek and Klomfar [74] for the NH_3+H_2O thermodynamic properties, here these properties are obtained instead using SAFT-γ Mie (with hydrogen properties evaluated using an ideal-gas model in all cases), allowing consideration of more organic working fluids comprised of different functional groups. For model validation the heat-input range, $150\,W \leq \dot{Q}_{gen} \leq 500\,W$, was considered. The model was also compared against experimental data for an NH_3—H_2O—H_2 DAR module operating at 17 bar charge pressure and cooling delivery at 5 °C, provided by Freeman et al. [12].

The comparison in Fig. 4 shows acceptable agreement with DAR simulations incorporating the correlations of Pátek and Klomfar, as well as with the experimental measurements (within ± 7%) for $150\,W \leq \dot{Q}_{gen} \leq 500\,W$, charge pressure of 17 bar and cooling-delivery temperature (cold-space temperature) of 5 °C. In this study, the maximum COP was reported as 0.24 at a generator heat input of about 300 W, beyond which the effectiveness of various components limits the COP (*e.g.*, the rectifier, the condenser and the evaporator). It can also be observed in Fig. 4, that heat dissipations from the bubble pump, rectifier, condenser, and absorber, calculated using the presented model, are comparable to those obtained using the Starace and De Pascalis model [26].

The quality of the presented DAR thermodynamic model is further assessed by expanding the experimental data set. Experimental DAR data for NH_3—H_2O—H_2 obtained from Najjaran [121] were used as inputs in calculations representing various operating conditions: three pressure levels (15 bar, 18 bar and 21 bar), and three charging compositions (25 wt.%, 30 wt.% and 38 wt.% refrigerant). Validation of the present framework was performed over a heat-input range $150\,W \leq \dot{Q}_{gen} \leq 500\,W$. In addition, further validation of the present framework, for the *i*-C_4H_{10}—*n*-C_8H_{18}—He system, is presented here, over a range of generator temperature, T_2, from 114 °C to 168 °C, using input data taken from Refs. [8,40].

In Fig. 5, parity plots of calculated and experimentally determined COP for the sets of data mentioned above are presented to demonstrate the model's applicability. For NH_3—H_2O—H_2, the model average deviation between the calculated and measured COP is ±0.036, which corresponds to an average deviation between calculated and measured cooling rate of 10 W or %AAD of ± 26%. One can discern from Fig. 5(a) that most COP data for NH_3—H_2O—H_2 fall between 0.1 and 0.2. The model performs better at the two lower pressure levels (15 bar and 18 bar), especially when the heat input is not low. The model predictions deviate less from the experimental data for the *i*-C_4H_{10}—*n*-C_8H_{18}—He system. The model average deviation in this case is ± 0.009 (as seen in Fig. 5(b)) corresponding a deviation of only 0.6 W or %AAD of ± 6%.

2.5.2. CAMD MINLP optimisation algorithm

Before demonstrating the MINLP optimisation results of the complete CAMD-DAR framework shown in Fig. 2, a series of parametric NLP and MINLP optimisations were performed. These parametric NLP and MINLP optimisations maximise the cooling rate, $\dot{Q}_{evap}$ for some organic-family combinations. For validation, a cooling temperature, T_{co} of 4 °C, was considered, which resembles an average cabin temperature in a household fridge. Three ambient temperature, T_a levels were used for validation: 20 °C, 30 °C and 40 °C, to cover a wide range of temperatures for regions where DAR is intended to be used. For obvious reasons, the gradient-based SQP optimisation algorithm is deployed instead of the OAERAP algorithm in the set of parametric NLP optimisations used for model validation.

The parametric MINLP optimisation results for aliphatic working fluids are compared to the results obtained from NLP optimisations, and the comparison is shown in Fig. 6. For each organic working-fluid combination, the optimal working fluid identified by the MINLP optimisation coincides with the best working fluid identified using NLP optimisations, except for 1-alkene—1-alkene (*i.e.*, 1-C_nH_{2n}—1-C_nH_{2n}) working-fluid mixtures. The working fluid identified by NLP optimisation for the three considered ambient temperatures is (C_3H_6—1-C_7H_{14}—He). On the other hand, the optimum working fluids suggested by the MINLP are 1-C_4H_8—1-C_9H_{18}—He for T_a = 20 °C and 1-C_4H_8—1-C_8H_{16}—He for T_a = 30 °C and 40 °C. Interestingly, these working fluids identified through MINLP optimisations correspond to 34 %, 59 % and 99 % more cooling than that identified through NLP optimisations. Hence, it can be verified that the parametric MINLP optimisations converge to the best optima. It is found that increasing the number of initial guesses (using multi-start optimisation) beyond 120 initial guesses does not improve the optimum DAR design for the investigated working-fluid combinations. Nevertheless, 500 initial guesses were used to ensure convergence, especially when investigating polar wroking fluids.

3. Results and discussion

The CAMD-DAR framework presented in Fig. 2 was implemented and different DAR designs are presented for both case studies described

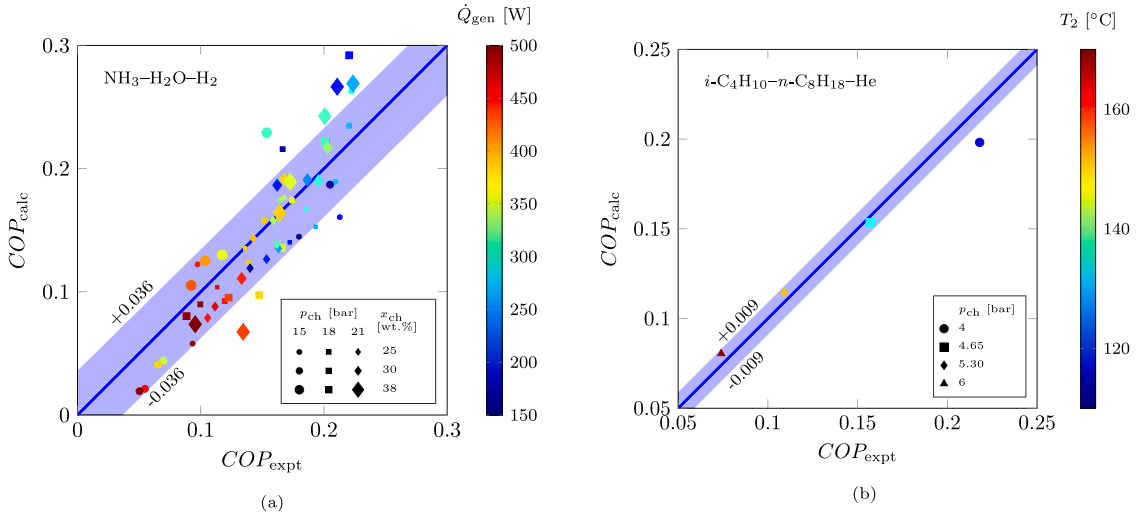

Fig. 5. Validation of the DAR model against: (a) NH_3—H_2O—H_2 DAR experiments performed by Najjaran [121]; and (b) simulations by Lee et al. [40] on a commercial i-C_4H_{10}—n-C_8H_{18}—He DAR module. The NH_3—H_2O—H_2 system in (a) delivers cooling at 5 °C at three different charging pressures (15 bar, 18 bar and 21 bar), three different charging compositions (25 wt.%, 30 wt.% and 38 wt.%) and variable supplied heat rates (150 W to 500 W); COP predictions made using this model lie within ± 26%. The i-C_4H_{10}—n-C_8H_{18}—He module considered in (b) is powered by a generator delivering 70 W and charged with 17 wt.% refrigerant-rich solution, at four charging pressures (4 bar, 4.65 bar, 5.30 bar and 6 bar) and a variable generator temperature (114 °C to 168 °C); COP predictions made using the model lie within ±6.4% of the experimental estimates. Symbol sizes reflect the variation of charging compositions, symbol colours map generator heat input in (a) and generator temperature in (b), and symbol shapes represent different charging pressures.

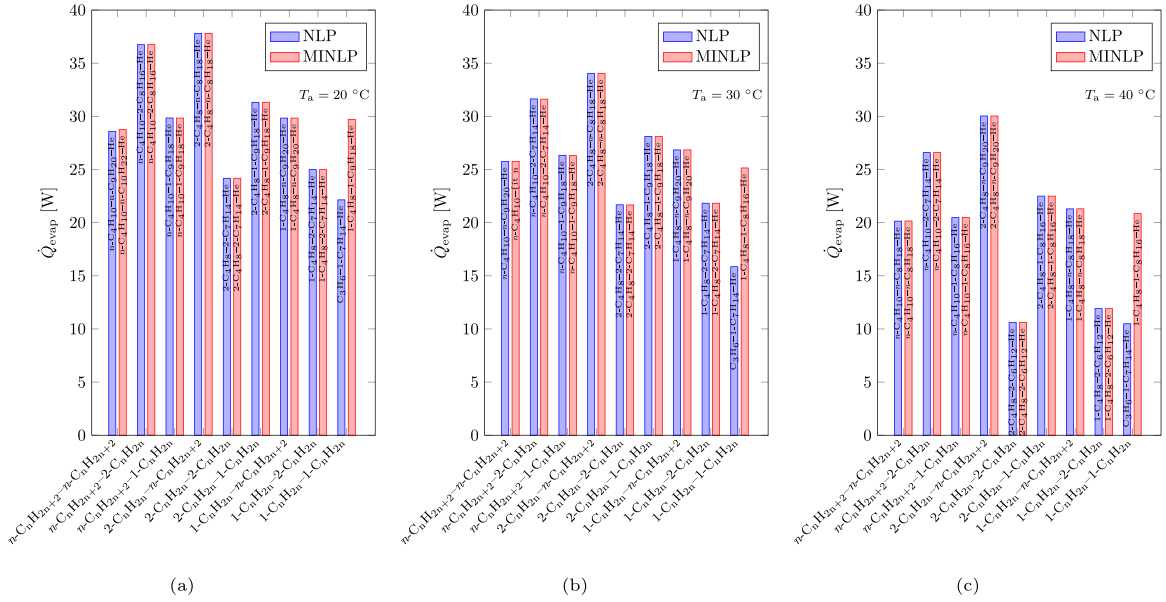

Fig. 6. Comparison of MINLP and NLP results for selected refrigerant and absorbent families.

in Section 2. The suggested optimum designs integrate the design of a working-fluid mixture (refrigerant, absorbent, and auxiliary gas), with the optimisation of other DAR operating conditions such as charging pressure, refrigerant-rich solution charging composition, and module size. Further, the results of multi-objective optimisation are presented.

3.1. Case study 1: Non-polar organic working-fluid design via MINLP optimisations

Optimisation results for the first case study (involving straight-chain non-polar working-fluid mixtures) are presented in Table 5. The rankings of best working fluids obtained from the MINLP and NLP optimisations compare well within the first six optimum alternatives. It should be recalled that the hybrid stochastic-deterministic optimisation method used in this study attempts to solve the optimisation problem as many times as the number of initial guesses provided, while these initial guesses (apart from the very first one) are randomly generated by the solver using a Sobol algorithm. Thus, the MINLP problem is solved as often as the solver succeeds in converging to an optimal solution. Employing an adequate number of initial guesses ensures not only reaching a non-dominated optimal solution but also a list of alternative optimal working fluids; thus, it is not necessary to employ integer cuts to explore new alternatives.

It can also be observed in Table 5 that $\tilde{x}_{rs} \leq 14$ %. It should be recalled that these low compositions are constrained by the limits on the weak-solution compositions imposed via Eqs. (10a) and (10b) to ensure proper absorption in the absence of a detailed absorber model,

Table 5
Ranking of optimum working fluids for cooling temperature, T_{co} = 4 °C and ambient temperature, T_a = 20 °C. Working-fluid pairs are sorted in descending order according to optimum cooling rates, $\dot{Q}_{evap}$.

MINLP Rank	NLP Rank	Working fluid	$\dot{Q}_{evap}$ [W]	$\dot{Q}_{gen}$ [W]	p_{ch} [bar]	$\tilde{x}_{rs}$ [mol %]	$\bar{T}_{gen,w}$ [°C]	$C_{CU,0}$ [£]	SPC [£W^{-1}]
1	1	2-C_4H_8—n-C_8H_{18}—He	37.8	250	2.7	14	107	787	20.87
2	2	2-C_4H_8—n-C_8H_{18}—H_2	36.6	261	2.9	13	107	806	22.04
3	3	2-C_4H_8—n-C_9H_{20}—He	36.5	313	2.7	13	132	645	24.60
4	5	2-C_4H_8—n-C_9H_{20}—H_2	36.5	344	3.2	12	132	897	25.96
5	6	n-C_4H_{10}—2-C_8H_{16}—H_2	36.3	240	2.6	14	112	768	21.15
6	4	n-C_4H_{10}—2-C_8H_{16}—He	35.9	257	3.0	13	112	800	22.30

Table 6
Results of parametric MINLP optimisations considering the first case study for T_a = 20 °C and T_{co} = 4 °C with three different objectives to: maximise the cooling rate, $\dot{Q}_{evap}$; minimise the purchase cost, $C_{CU,0}$; and minimise the specific purchase cost of cooling, SPC.

Objective function	Working fluid	$\dot{Q}_{evap}$ [W]	$\dot{Q}_{gen}$ [W]	p_{ch} [bar]	$\tilde{x}_{rs}$ [mol %]	$\bar{T}_{gen,w}$ [°C]	$C_{CU,0}$ [£]	SPC [£W^{-1}]
max $\dot{Q}_{evap}$	2-C_4H_8—n-C_8H_{18}—He	37.8	250	2.7	14	107	787	20.87
min $C_{CU,0}$	2-C_4H_8—2-C_6H_{12}—He	5.3	50	3.3	14	101	309	61.89
min SPC	2-C_4H_8—n-C_6H_{14}—He	30.5	132	2.2	16	69	544	17.81

which is outside the scope of this study. Bounded weak-solution compositions drive the optimisations towards less charging compositions. The reported compositions agree well with theoretical and experimental charging compositions reported for similar absorption–refrigeration systems operating with similar organic working fluids [8,40,41]. It can also be observed that all refrigerants in Table 5 contain four carbon atoms, while the optimum absorbents contain either eight or nine.

The objective function can shape the working-fluid selection and the DAR system design. To assess the effect of the objective function, MINLP optimisations are performed solving Eq. (5) but for two other objective functions, minimising the purchase cost, $C_{CU,0}$ and minimising the specific purchase cost of cooling, SPC. When $C_{CU,0}$ is minimised, the performance of the DAR module is controlled by the bubble pump constraints Eqs. (7a) to (7c).

Different objective functions are compared in Table 6. The results in this table establish that the refrigerant selection is not affected by the change in the objective function; 2-C_4H_8 is the optimum refrigerant for all objective functions studied. Conversely, absorbent selection depends on the objective function. When maximum $\dot{Q}_{evap}$ is called, the optimum absorbent is n-C_8H_{18}, while if minimum $C_{CU,0}$ is called, 2-C_6H_{12} is selected as the optimum absorbent; n-C_6H_{14} is promoted as the optimum absorbent for minimum SPC. It can be realised that DAR design variables ($\dot{Q}_{gen}$, p_{ch} and $\tilde{x}_{rs}$) marginally depend on the objective function.

Clearly, for minimum $C_{CU,0}$, the MINLP converges towards the smallest DAR size characterised by its supplied heat rate, $\dot{Q}_{gen}$ (50 W), whereas, when SPC is minimised, the DAR size (132 W) falls between the largest DAR for maximum $\dot{Q}_{evap}$ (250 W) and the size for minimum $C_{CU,0}$ (50 W). The DAR design for minimum SPC coincides with that if the COP is maximised. In the present framework, $C_{CU,0}$ calculated using Eq. (4) is a function of $\dot{Q}_{gen}$ only. Thus, minimising SPC is almost the same problem as maximising the COP, which has been confirmed by running the MINLP for maximum COP. Notably, SPC is the highest for the system with the minimum $C_{CU,0}$.

From Table 6, it can also be seen that the optimisation objective influences less the rich-solution composition; nonetheless, it is more influenced by the absorption affinity constraint in Eq. (10b) and the working fluid. Interestingly, the predicted generator temperature is the lowest for the system with a minimum SPC ($\bar{T}_{gen}$ = 69 °C) due to the low charge pressure and rich-solution composition required to charge the system.

The results in Table 6 emphasise the importance of considering the trade-off between maximising the cooling rate and minimising the purchase cost of the DAR module. The MINLP optimisations offer alternative working fluids that can perform as well as standard DAR modules with NH_3—H_2O in terms of $\dot{Q}_{evap}$. Moreover, the optimisations suggested working fluids that can be generated with relatively lower temperatures compared to those required by NH_3—H_2O DAR modules.

A sensitivity analysis based on the elementary-effect method has been carried out to quantify the effect of different decision variables on the prediction of cooling rates, revealing that the most influential variable in this context is $n_{CH_2,refr}$, the number of methylene groups in the refrigerant molecule. Full discussion of this analysis is provided in a Supplementary Material file.

3.2. Case study 2: Considering branched and polar organic working fluid for small-scale DAR modules

In Fig. 7, for a 283 L DAR module (≈ 440 W rated supplied heat rate), four optimum working-fluid mixtures can be identified for maximum cooling rates over the range of considered ambient and cooling temperatures. Notably, the refrigerants in these four working fluids are non-polar hydrocarbons: 2-butene (2-C_4H_8); 1-butene (1-C_4H_8); propane (C_3H_8) and 4-methyl,2-pentene ([CH_3]$_2$>CHCH=CHCH$_3$). On the other hand, optimum absorbents tend to contain a polar group. For the considered temperature space, the identified absorbents are limited to: ethanol (C_2H_5OH); 1-aminopropylene (CH_3CH=$CHNH_2$); aminoethylene (CH_2=$CHNH_2$) and 1-aminobutadiene (CH_2=$CHCH$=$CHNH_2$). Unsurprisingly, helium is elected as the auxiliary gas in all the optimisations. Pressuring organic-based DAR modules can be safer using helium than hydrogen. The latter might become reactive with some organic compounds at high temperature and pressure.

From Fig. 7(a), it can be demonstrated that optimum cooling rates monotonically decrease as ambient temperature increases or cooling temperature decreases. It is also revealed that, thermodynamically, 2-butene—ethanol—helium (2-C_4H_8—C_2H_5OH—He) offers an optimum working fluid for a wide range of ambient and cooling temperatures (*i.e.*, 20 °C ≤ T_a ≤ 40 °C and −4 °C ≤ T_{co} ≤ 8 °C) with cooling rates ranging between 70 W and 154 W.

The working fluid, 1-butene—1-aminopropylene—helium (1-C_4H_8—CH_3CH=$CHNH_2$—He) is identified by the CAMD-DAR framework to be the optimum working fluid for very low cooling temperatures (T_{co} ≃ −18 °C) and high ambient temperatures (T_a ≥ 30 °C), which makes it the right choice for applications for food freezing in remote hot regions such as Sub-Saharan Africa or the Gulf region where a 283 L

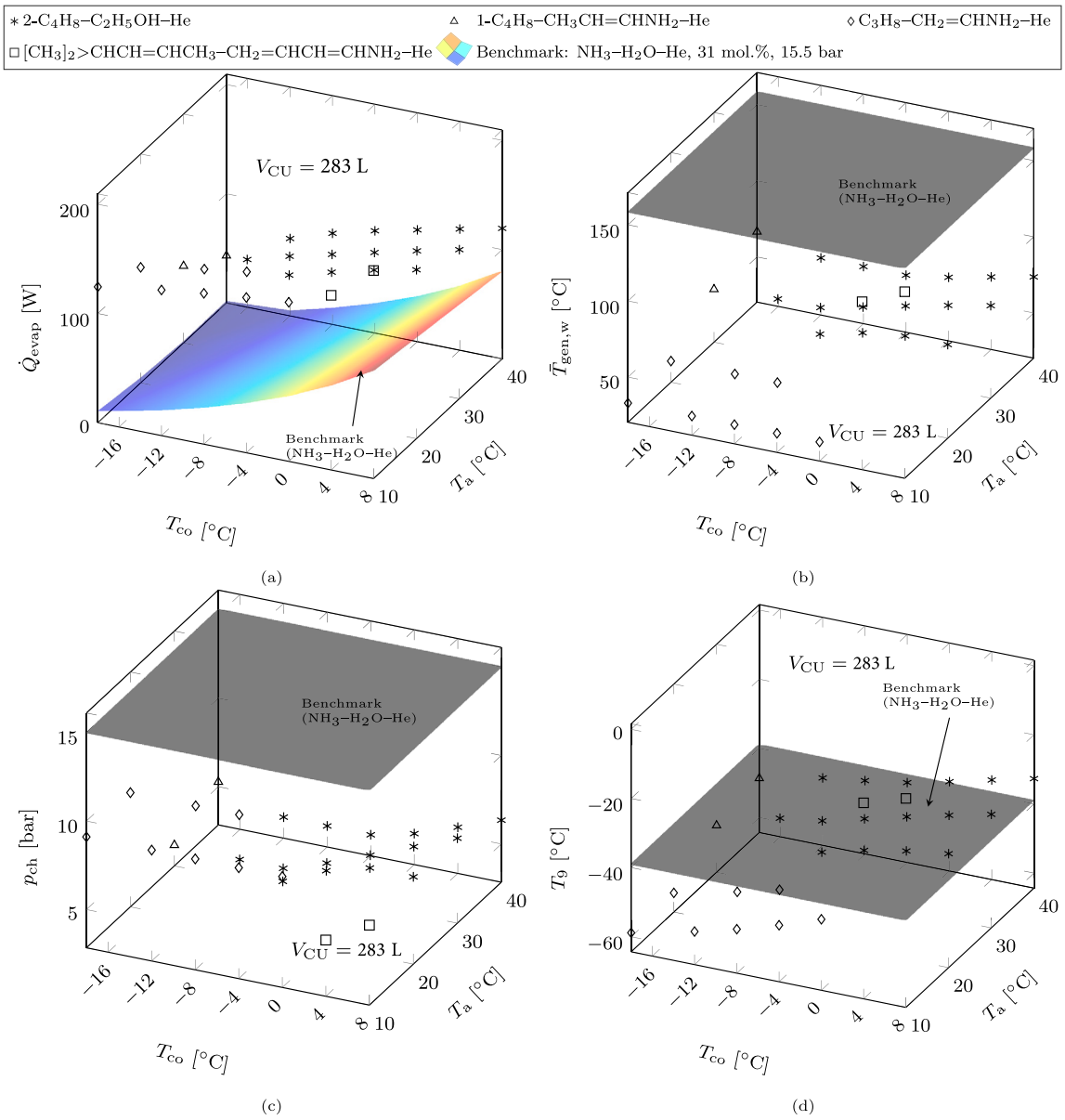

Fig. 7. Mapping results of the MINLP CAMD-DAR problem described in Eq. (5) to design optimal organic working-fluid mixtures and corresponding charging settings for a 283-L DAR module (corresponding to ≈ 440 W supplied heat rate) over a wide range of ambient and cooling temperatures. The optimal systems are compared to an NH_3–H_2O DAR module charged with 31 mol % rich solution at 15.5 bar described by the surface plots: (a) cooling rate, $\dot{Q}_{evap}$; (b) DAR generator temperature, $\bar{x}_{rs}$; (c) DAR charge pressure, p_{ch} and (d) lowest temperature in the evaporator, T_9.

DAR module running with 1-C_4H_8—CH_3CH=$CHNH_2$—He can provide theoretical cooling rates of 43 W to 70 W depending on the operating conditions. Contrarily, propane—aminoethylene—helium (C_3H_8—CH_2=$CHNH_2$—He) is recommended for lower ambient temperatures ($T_a \leq 20$ °C) and a wide range of low cooling temperatures ($T_{co} < 0$ °C) with cooling rates ranging from 105 W to 146 W. 4-methyl,2-pentene—1-aminobutadiene—helium ($[CH_3]_2$>CHCH=CH CH_3—CH_2=CHCH=$CHNH_2$—He) is identified as an optimum working fluid for $T_{co} = 8$ °C and $T_a = 10$ °C.

The results in Fig. 7(a) also reveal that all the suggested optimum working fluids are deemed to produce more cooling than the benchmark NH_3—H_2O DAR module by more than 50%. It can be observed in Fig. 7(b) that the required generator wall temperatures to generate the rich-solution 45 °C to 155 °C, for most of the proposed working fluids, are much less than the generation temperature required for NH_3—H_2O.

Further, from Fig. 7(c), the theoretical charge pressure required by each of the optimum DAR modules for maximum cooling is much less than 15.5 bar ($4 \leq p_{ch} \leq 9.5$ bar). Lower charging pressure reduces the generator's load, promotes a higher cooling rate, and ensures safer operation, provided that this pressure is sufficient to ensure complete condensation of the corresponding refrigerant at all operating ambient temperatures. From Fig. 7(d), it can be revealed that for the suggested optimum DAR designs, the temperature drop resulting from the adiabatic mixing of refrigerant and auxiliary gas is, in most cases, comparable to evaporator temperatures in the NH_3—H_2O DAR module considered for comparison. Low evaporator temperatures allow multi-purpose operation (*e.g.*, freezing and refrigeration), as long as the lowest temperature in the evaporator is above the refrigerant's freezing point, a condition which is met for all proposed working-fluid mixtures.

Generally, it can be concluded that small-sized non-polar refrigerants are favoured due to their relative volatility compared to polar

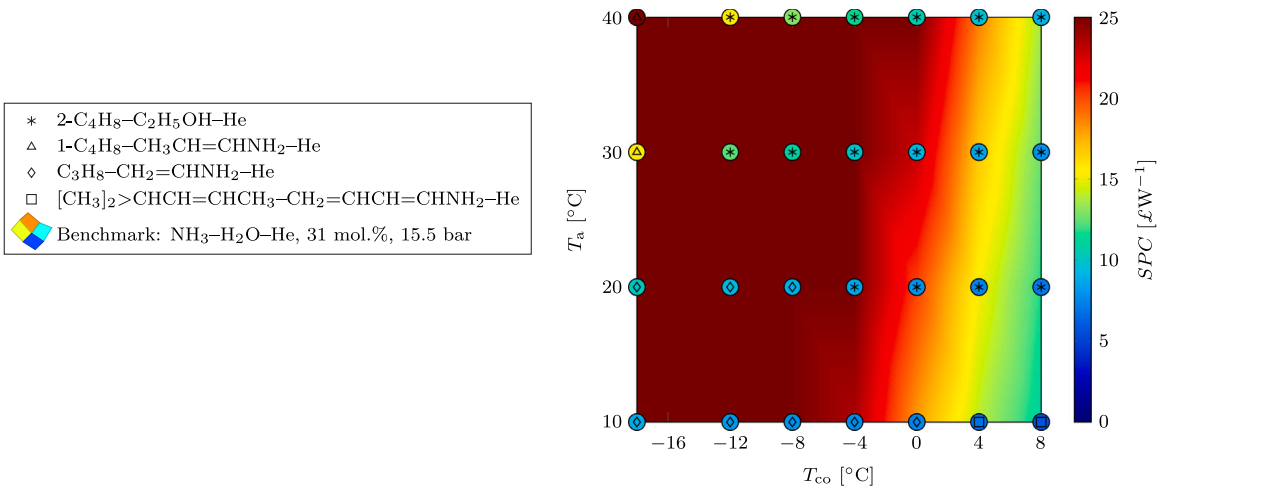

Fig. 8. Effect of ambient temperature and cooling temperature on SPC for optimal organic working-fluid mixtures and corresponding charging settings presented in Fig. 7, where a 283 L DAR module (corresponding to ≈ 440 W supplied heat rate) is considered. The optimal systems are compared to the SPC predicted for the benchmark NH_3–H_2O DAR module charged with 31 mol % rich solution at 15.5 bar described by the surface plot.

molecules of the same carbon-chain length. Results in this case study combined with results presented in Section 3.1 suggest that 2-alkenes and branched hydrocarbons offer higher cooling capacity compared to *n*-alkanes due to their higher latent heat of vaporisation, which makes them preferred choices as a refrigerant. This observation agrees with results [58,59] for designing working fluids for ORC systems, and the study published by Papadopoulous et al. [60], in which working-fluid mixtures are considered for optimum absorption refrigeration system design. On the other hand, it can be observed that polar (*e.g.*, alcohols or amines) are preferred to non-polar molecules (*e.g.*, hydrocarbons) as absorbents. When we couple non-polar refrigerants with polar absorbents the less-volatile nature of the polar absorbent increases the relative volatility of the refrigerant–absorbent pair at the generator temperature (compared with a non-polar pair), making it easier to rectify the refrigerant, and may eliminate the need for the rectifier.

Further, as can observed in Fig. 7(a), the CAMD-DAR framework suggests the elected working fluids can produce cooling with COP exceeding 0.35, especially in low ambient conditions. It is worth mentioning that the cooling rate (and also the COP) deteriorates as the ambient temperature increases. The COP also significantly diminishes as the cooling temperature decreases.

In order to complement the thermodynamic analysis presented above, the specific cooling cost, SPC for optimum DAR modules of 283 L size (corresponding to ≈ 440 W supplied heat rate) is presented in Figs. 8 and 9. The specific cooling costs, SPCs (Eq. (6)), for optimum DAR designs identified in Fig. 7 are mapped in Fig. 8. It can be observed that the considered NH_3—H_2O DAR module demonstrates a relatively high SPC compared to the organic working fluids proposed in Section 3.1 and this section. As the cooling temperature decreases, SPC increases exponentially.

It can also be realised from Fig. 8 that for the considered NH_3—H_2O DAR module, SPC is less affected by the ambient temperature variation than the cooling-temperature effect. It can be easily recognised that, compared to the NH_3—H_2O DAR module, the optimum DAR designs suggested by the CAMD-DAR framework can offer lower SPC. For example, for 20 °C ambient temperature and 4 °C cooling temperature, the optimum DAR module charged with 2-C_4H_8—C_2H_5OH—He is predicted to have an SPC of £ 7.46 per W, which is 50 % less than the anticipated SPC of using the benchmark NH_3—H_2O DAR module for the same ambient and cooling temperatures. It can be observed that the organic working fluids presented in the second case study offer lower SPC than simple working fluids considered in this paper.

Following the discussion presented above, the required generator temperature $\bar{T}_{gen,w}$, and the SPC for the four optimal fluids identified in Fig. 7 are plotted in Fig. 9 against various DAR sizes for which the cooling rate is maximised considering ambient and cooling temperatures of 20 and 4 °C, respectively. It can be observed that generator temperatures required for the organic working fluids are less than those for NH_3—H_2O. It can be noted from Fig. 9(b) that all the proposed fluids can result in 15 % to 50 % reduction in predicted SPC compared to a benchmark NH_3—H_2O DAR module of the same size. Similar to the earlier discussion, it can be revealed from this figure that a 170 L DAR module charged with 1-C_4H_8—CH_3CH=$CHNH_2$—He has the lowest SPC of £ 7.1 per W, which is 55 % less than SPC of an NH_3—H_2O DAR module of the same size and 3 % less than SPC of the 283 L DAR module charged with 2-C_4H_8—C_2H_5OH—He (for which the cooling rate is maximised).

As discussed in Section 3.1, an advantage of using multi-start hybrid stochastic-deterministic optimisation methods, such as the one deployed in this study, is that it can provide a list of sorted alternative optimal solutions without the need to apply integer cuts. For example, the best ten integrated DAR designs generated by the CAMD-DAR framework for the 283 L DAR module operating at T_a = 20 °C to deliver cooling at T_{co} = 4 °C are presented in Table 7. It can be noted that for maximum cooling using a 440 W thermally powered DAR module, 2-C_4H_8—C_2H_5OH—He is the optimum working fluid. offering cooling rate up to 146 W (corresponding to COP = 0.33). The required generator temperature for this design is as low as 82 °C, which is promising for non- or low-concentrating solar-thermal collector applications. The 2-C_4H_8—C_2H_5OH—He DAR module needs a charge pressure of 7.1 bar. The produced cooling hence comes at a specific cost of £ 7.46 per W.

It can be observed that the CAMD-DAR framework selects some inferior polar refrigerants. For instance, for T_a = 20 °C and T_{co} = 4 °C, the third-best working fluid contains aminoethylene ($C_2H_5NH_2$) as the refrigerant, with a primary amine group (–NH_2), while the fourth-best working fluid contains di-methylamine (CH_3NHCH_3) as the refrigerant, with a secondary amine group (>NH). It can also be observed that none of the refrigerants in the first ten optimal solutions (actually, none at all) are alcohols.

The CAMD-DAR framework suggests that alcohols cannot be used as refrigerants, limited by the ability of the generator to initiate the bubble pump to circulate alcohol-based DAR modules. However, simple alcohols (*i.e.*, methanol and ethanol) can be used as refrigerants with some ionic-liquid absorbents for conventional absorption refrigeration systems as evaluated by Boman et al. [122] although, due to the passive

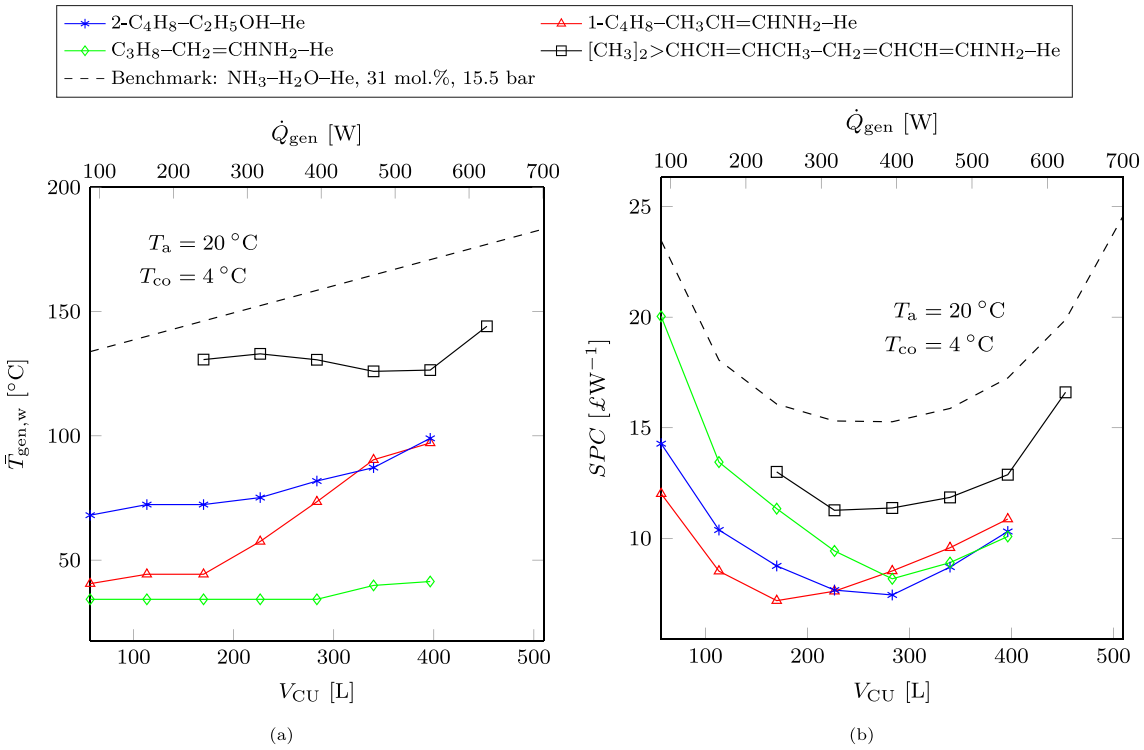

Fig. 9. Effect of optimised DAR size on required generator temperature (a), and specific purchase cost of cooling, SPC (b), for four working fluids identified in Fig. 7, corresponding to maximum cooling rates. NLP optimisations are considered for (T_a = 20 °C and T_{co} = 4 °C). Optimum cooling rates and optimised variables are compared against the benchmark NH_3—H_2O DAR module described above.

Table 7
Results of MINLP optimisations for the second case-study (283-L DAR module ($\dot{Q}_{gen}$ = 440 W) with T_a = 20 °C and T_{co} = 4 °C). Helium is identified as the auxiliary gas for all the presented working fluids. Rank refers to the order in which the multi-start optimiser sorts the optimal solutions; two optimal solutions are the same if their objective function values and arguments are similar within 1%.

Rank	Refrigerant	Absorbent	$\dot{Q}_{evap}$ [W]	p_{ch} [bar]	$\bar{x}_{rs}$ [mol %]	$\bar{T}_{gen,w}$ [°C]	SPC [£W^{-1}]
1	2-C_4H_8	C_2H_5OH	146	7.77	14	82	7.46
2	1-C_4H_8	$CH_3CH{=}CHNH_2$	128	6.12	13	73	8.51
3	$C_2H_5NH_2$	$CH_2{=}CHCH{=}CHNH_2$	120	4.75	13	102	9.09
4	CH_3NHCH_3	$C_2H_5CH{=}CHNH_2$	113	8.36	13	77	9.64
5	2-C_4H_8	$CH_2{=}CHCH{=}CHNH_2$	100	3.61	13	94	10.90
6	$[CH_3]_2$>$CHCH{=}CHCH_3$	$CH_2{=}CHCH{=}CHNH_2$	96	6.02	13	131	11.35
7	1-C_4H_8	$CH_2{=}CHCH_2OH$	96	4.83	13	90	11.35
8	$[CH_3]_2$>$CHCH{=}CH_2$	2,4-C_6H_{10}	89	4.73	12	100	12.24
9	1-C_4H_8	$CH_2{=}CHCH[CH_2]_2NH_2$	78	3.97	13	70	13.97
10	i-C_4H_{10}	$[CH_3]_2$>$CHOH$	76	6.7	13	104	14.33

nature of DAR cycles, in contrast to absorption–refrigeration cycles, the choice of refrigerant–absorbent pair is found to be limited by the bubble-pump operation.

It can also be noticed in Table 7, a rare example of a non-polar organic pair is identified: a mixture of 3-methylbutene ($[CH_3]_2$>$CHCH{=}CH_2$) as the refrigerant and 2,4-hexadiene (2,4-C_6H_{10}) as the absorbent. 3-methylbutene is a branched alkene with a single terminal double bond and five carbon atoms, while 2,4-hexadiene is a linear alkene with two internal double bonds. The comparison between the optimal working fluids identified in Tables 5 and 7 suggests that complex hydrocarbon systems which have polar absorbents are more thermodynamically favoured for maximising the cooling rates. Unsurprisingly, most of the selected refrigerants have four carbon atoms, which agrees well with the results presented in Section 3.1. These results collectively suggest the advantage of having olefin refrigerants to maximise the cooling rate. It can also be demonstrated that helium is thermodynamically more favourable than hydrogen as the auxiliary gas.

The integrated CAMD-DAR framework (listed in Table 3) incorporates limitations to ensure that optimised DAR modules comply with environmental and safety regulations. The global-warming and ozone-depletion-potential (GWP and ODP) restrictions ensure that a working fluid is environmentally friendly. The GWP of refrigerants and absorbents is limited by 150 as an upper bound; [56] many refrigerants and absorbents considered have almost zero GWP. In this study, the ODP should not exceed 0.2. However, it can be revealed that for a stricter limit, allowing only zero-ODP molecules to be considered, none of the presented refrigerants would be selected. It should be mentioned that should fluorinated, and hydrofluorinated groups be considered, GWP and ODP can play a more significant role in designing the working fluid.

For safe DAR operation, it is important to ensure that the working fluid is not ignitable and less likely to burn at the risk of any leakage. All the designed refrigerants have high LC_{50} to ensure they are not

Table 8
Results of parametric MINLP optimisations considering the second case study for T_a = 20 °C and T_{co} = 4 °C with three different objectives to: maximise the cooling rate, $\dot{Q}_{evap}$; minimise the purchase cost, $C_{CU,0}$; and minimise the specific purchase cost of cooling, SPC.

Objective function	Working fluid	$\dot{Q}_{evap}$ [W]	$\dot{Q}_{gen}$ [W]	p_{ch} [bar]	$\bar{x}_{rs}$ [mol %]	$\bar{T}_{gen,w}$ [°C]	$C_{CU,0}$ [£]	SPC [£W^{-1}]
max $\dot{Q}_{evap}$	2-C_4H_8—C_2H_5OH—He	148	412	7.1	14	77	1052	7.11
min $C_{CU,0}$	$[CH_3]_2$>CHCH=$CHCH_3$—CH_3CH=$CHNH_2$—H_2	50	2	14	14	106	309	21.43
min SPC	1-C_4H_8—CH_3CH=$CHNH_2$—H_2	121	282	3.9	15	51	845	6.97

toxic for handling and at risk of leakage. Only low-toxicity refrigerants and absorbents are selected. To avoid super-flammable working fluids, the flammability (Γ-) number, calculated using the method of by Kondo et al. [110] should not exceed 0.8. Unsurprisingly, most of the recommended working-fluid systems are strongly flammable ($0.6 \leq \Gamma \leq 0.8$). Polar refrigerants are favoured over non-polar refrigerants for being relatively less flammable but at the cost of reducing the cooling capacity. For the same reason, amine absorbents are favoured over alcohols for their lower Γ-number.

In addition, the designed refrigerants and absorbents have high enough auto-ignition temperatures compared to the predicted generator temperature. The maximum DAR power for a given working-fluid mixture is limited by minimum the auto-ignition temperature, T_{AIT}, of both the absorbent and the refrigerant (and the vapour-generation rate). For some working-fluid mixtures, especially those with n-C_nH_{2n+2}–n-C_nH_{2n+2} pairs, the theoretical temperature at the generator increases as the theoretical DAR power increases. Thus, the theoretical generator temperature tends to hit the safe bound of $T_{AIT,absr}$ described by the constraint in Eq. (19a). T_{AIT}, estimated using the GC method of Albahri et al. [109], decreases as the carbon-chain length increases thereby promoting the selection, within the CAMD-DAR framework, of shorter carbon-chain absorbents.

The results in Table 8 support the results in Table 6 on the importance of considering the trade-off between maximising the cooling power output and minimising the purchase cost of the DAR module. The presented set of MINLP optimisations offers alternative working fluids that can perform as well as standard DAR modules with NH_3—H_2O in terms of $\dot{Q}_{evap}$. Moreover, the optimisations suggested working fluids that can be generated with relatively lower temperatures compared to temperatures required by NH_3—H_2O DAR modules.

3.3. Multi-objective optimisations for small-scale DAR modules via MINLP optimisations

The importance of the trade-off between the purchase cost, $C_{CU,0}$ and theoretical cooling rate, $\dot{Q}_{evap}$ has already been discussed. The results presented in Tables 6 and 8 unleash this trade-off considering minimising the specific purchase cooling cost, SPC. Moreover, the selected optimum working fluid is found to be affected by the objective function considered, and the minimum SPC does not necessarily correspond to either maximum $\dot{Q}_{evap}$ or minimum $C_{CU,0}$.

In this section, two scenarios are considered. In both, the size of the DAR is a decision variable. In the first case, the size of the DAR module is identified by its supplied heat rate, $\dot{Q}_{gen}$ and is allowed to vary continuously; a continuous Pareto front, displayed in Fig. 10, is generated. In the second case, the size of the DAR module is identified by its rated volume, V_{CU} as available in the market, taking an integer value between 57 L and 283 L, and a discrete Pareto front, displayed in Fig. 11, is generated.

From Fig. 10, the best SPC is obtained by DAR modules with $\dot{Q}_{evap} \approx 120$ W running with 1-C_4H_8—CH_3CH=$CHNH_2$—He. This result matches the results displayed in Fig. 9, where 1-C_4H_8—CH_3CH=$CHNH_2$—He is identified to have the lowest SPC. It can also be observed that the minimum SPC is only 1% less than that for the working fluid with maximum $\dot{Q}_{evap}$.

The results in Fig. 10 reveal that 1-aminopropene (CH_3CH=$CHNH_2$) and allylamine (CH_2=$CHCH_2NH_2$, *aka* 1-amino-2-propene) are the most-selected molecules as absorbents. Although both aminopropenes passed environmental, toxicity and safety checks considered in this study, the National Center for Biotechnology Information [123] identifies allylamine as toxic with a low flash point, which implies that working fluids with allylamine should be considered with more caution. Short-chain alcohols are also recommended as absorbents by the MINLP optimisations. Unsurprisingly, it can be observed from Fig. 10 that all refrigerants that fall on the Pareto front are non-polar. It is also not surprising that most non-dominated DAR designs use helium as the pressurising gas though hydrogen can still be used.

The Pareto front in Fig. 10 gives an insight into which DAR design should be adopted. If high cooling rates > 100 W are required, then DAR modules with 2-C_4H_8—C_2H_5OH—He or 1-C_4H_8—CH_3CH=$CHNH_2$—He are recommended, while if low purchase cost is of interest, working fluids such as 1–C_4H_8—CH_3CH=$CHNH_2$—H_2 and 4-methyl-2-pentene—CH_3CH=$CHNH_2$—H_2, with the corresponding charging settings, are recommended.

When the decision variable describing the DAR-unit size is discretised, the Pareto front is reduced to the frontier displayed in Fig. 11. The minimum SPC is obtained by charging a 170 L DAR module with 1-pentane—1-aminopropylene—H_2 (1-C_5H_{10}—CH_3CH=$CHNH_2$—H_2), which differs from the optimal working fluid (1-C_4H_8—CH_3CH=$CHNH_2$—He) for minimum SPC identified in Fig. 10. The optimal SPC identified in Fig. 10 relates to a DAR module that receives 282 W, which lies between the supplied heat rates needed to operate 170 L and 227 L DAR cooling modules; the appropriate DAR size rounds to the larger size and hence the higher SPC. This explains why 1-C_4H_8—CH_3CH=$CHNH_2$—He is dominated by 1-pentane—1-aminopropylene—H_2 when the discretised space of DAR size is considered. It can be observed from Fig. 11 that 1-aminopropene dominates other absorbents except for the 283 L DAR module.

4. Conclusions

A CAMD-DAR framework for the design of optimal small-scale DAR modules was developed for solar-cooling applications, with a particular interest on the operation of such modules using low-temperature, *i.e.*, low-cost non- or low-concentrating solar-thermal collectors (50 °C to 150 °C). The framework simultaneously identifies optimal working-fluid mixtures and DAR-system designs, while considering an extensive variety of organic fluids comprised of a range of functional groups, including polar organic groups.

Using an otherwise conventional, small-scale DAR module design, single- and multi-objective MINLP optimisations were performed using the integrated CAMD-DAR framework to maximise cooling rate through working-fluid design and operational setting selection (*e.g.*, system pressure and fluid concentration) over a range of ambient (10 °C to 40 °C) and cooling (−16 °C to 8 °C) temperatures.

It has been demonstrated that non-polar+polar working-fluid mixtures are favoured for maximum cooling rates. For a 440 W thermally powered DAR module, cooling rates up to 146 W can be achieved for 4 °C cooling temperature if 2-C_4H_8—C_2H_5OH—He is used at a charge pressure of 7.1 bar. This design has a specific cost as low as

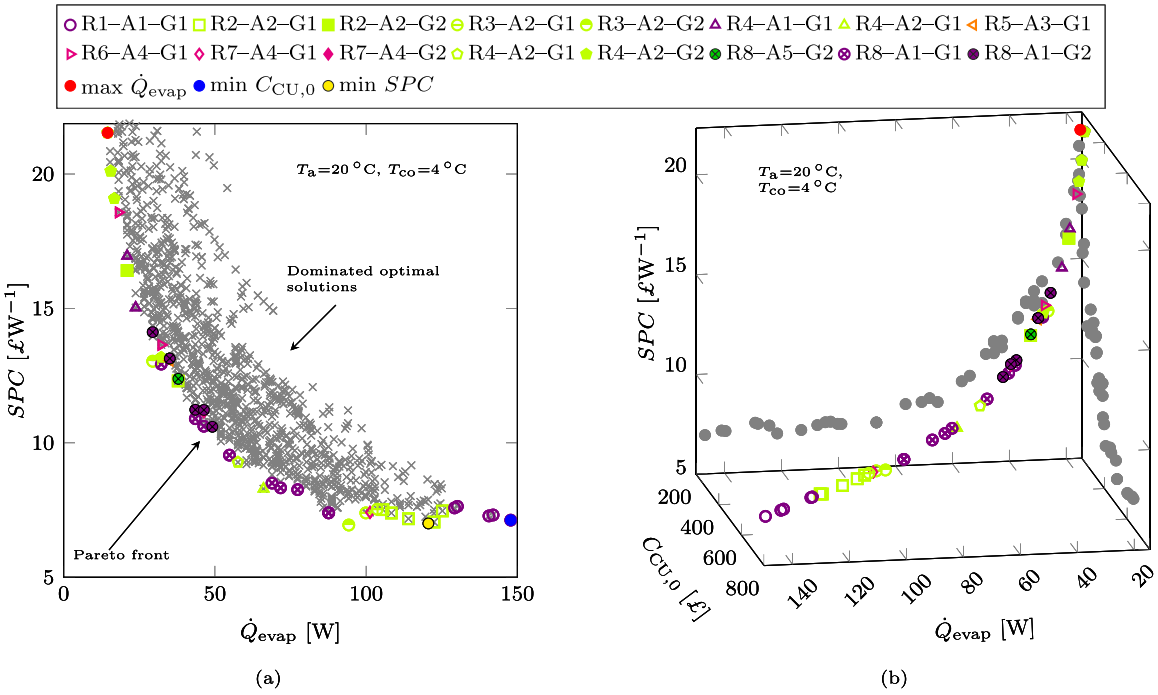

Fig. 10. Results of multi-essential optimisations for $\dot{Q}_{gen}$ as a continuous decision variable, ambient temperature, T_a = 20 °C and cooling temperature, T_{co} = 4 °C with two objective functions: max $\dot{Q}_{evap}$ and min $C_{CU,0}$. (a) SPC against $\dot{Q}_{evap}$ demonstrating dominated and non-dominated optimal solutions; (b) three-dimensional plot of $C_{CU,0}$ (x-axis) against $\dot{Q}_{evap}$ (y-axis) against SPC (z-axis), and 2D projections (in grey) of the Pareto front on $x-z$ and $y-z$ planes. Refrigerants are R1:2-C_4H_8, R2:1-C_4H_8, R3:1-C_5H_{10}, R4:[CH_3]$_2$>CHCH=CH_2, R5:2-C_5H_{10}, R6:*n*-C_4H_{10}, R7:*i*-C_4H_{10}, and R8:2-C_5H_{10}. Absorbents are A1:C_2H_5OH, A2:CH_3CH=$CHNH_2$, A3:1-C_3H_7OH, A4:CH_2=$CHCH_2NH_2$, and A5: CH_2=$CHCH_2OH$. Auxiliary gases are G1:He, and G2:H_2.

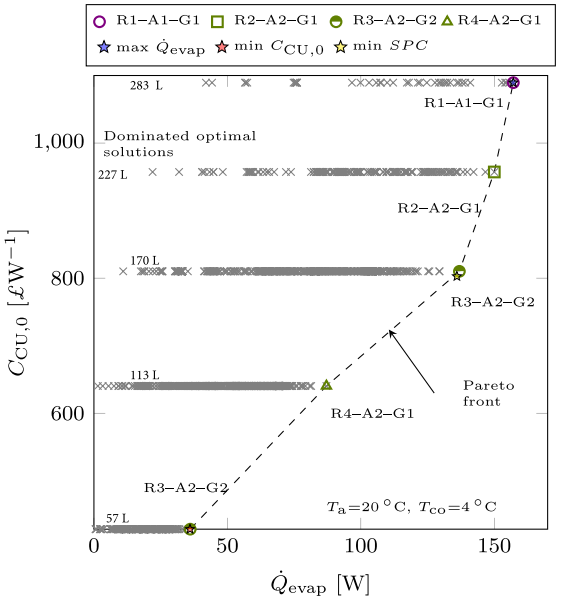

Fig. 11. Results of multi-objective optimisations for V_{CU} as an integer decision variable, ambient temperature, T_a = 20 °C and cooling temperature, T_{co} = 4 °C with two objective functions: max $\dot{Q}_{evap}$ and min $C_{CU,0}$ demonstrating dominated and non-dominated optimal solutions. Refrigerants are R1:2-C_4H_8, R2:1-C_4H_8, R3:1-C_5H_{10}, and R4:[CH_3]$_2$>CHCH=CH_2. Absorbents are A1:C_2H_5OH, and A2:CH_3CH:$CHNH_2$. Auxiliary gases are G1:He, and G2:H_2.

£ 7.46 per W of cooling, and COP of 0.33 when operated at an ambient temperature of 20 °C. This design requires an 82 °C heat source, which make it a suitable design to be powered using non- or low-concentrating solar-thermal collectors. Notably, the coefficient of performance significantly diminishes as the cooling temperature decreases. The COP also decreases as the ambient temperature goes up. Other sub-optimal working fluids and corresponding DAR charging settings have also been identified. Most identified refrigerants have 3 to 5 carbon atoms. In addition, olefin refrigerants are preferred for their higher latent heat and thus cooling rates.

Compared to an NH_3—H_2O DAR module, the DAR module based on 2-C_4H_8—C_2H_5OH—He provides more cooling at a lower specific cooling cost. Interestingly, the required generator temperatures for optimum organic working fluids can be much lower than those needed to activate the NH_3—H_2O DAR module. All the identified working-fluid mixtures are environmentally friendly in terms of avoiding carbon emissions, but many refrigerants are flammable, with flammability numbers between 0.6 and 0.8.

Further, multi-objective optimisation highlights the trade-off between maximising the cooling rate, $\dot{Q}_{evap}$ and minimising the purchase cost, $C_{CU,0}$ to obtain a set of non-dominated design alternatives. Results from multi-objective optimisations suggest that 1-aminopropene (CH_3CH=$CHNH_2$) and allylamine (1-amino-2-propene or CH_2=$CHCH_2NH_2$) are the most-selected molecules as absorbents on the Pareto front. In contrast, all non-dominated refrigerants are non-polar. The Pareto front generated using the multi-objective optimisation provides a powerful tool for selecting a DAR module based on the relative importance of the cost and cooling rate.

The presented CAMD-DAR framework can be extended by introducing more organic groups and environmental and safety constraints. The framework can also be upgraded by expanding the multi-objective optimisation to include more independent objective functions to involve environmental objectives.

Table A.1
Fundamental DAR-thermodynamic mathematical model equations founded in the first-law of thermodynamics as used in this thesis.

Generator	$\dot{m}_1 = \dot{m}_2 = \dot{m}_{rs}$,	(Total material balance)	(A.2a)
	$\dot{m}_1\hat{h}_1 + \dot{m}_5\hat{h}_5 + \dot{Q}_{gen} = \dot{m}_4\hat{h}_4 + \dot{m}_{ws,in}\hat{h}_{ws,in} + \dot{Q}_{bp}$	(Energy balance – fully attached bubble pump)	(A.2b)
	or		
	$\dot{m}_1\hat{h}_1 + \dot{Q}_{gen} = \dot{m}_2\hat{h}_2$.	(Energy balance – semi-attached bubble pump)	(A.2c)
Bubble pump	$\dot{m}_2 = \dot{m}_3 + \dot{m}_4$	(Total material balance)	(A.3a)
	$\tilde{x}_{rs}\dot{m}_2 = \tilde{x}_3\dot{m}_3 + \tilde{y}_4\dot{m}_4$	(Refrigerant material balance)	(A.3b)
	$\{x_3, y_4\} = f(T_4, p_4, x_{rs})$	(VLE)	(A.3c)
	$\dot{Q}_{bp} = \dot{m}_2\hat{h}_2 - \dot{m}_3\hat{h}_{L,3} - \dot{m}_4\hat{h}_{V,4}$	(Energy balance)	(A.3d)
Rectifier	$\dot{m}_4 = \dot{m}_5 + \dot{m}_6$	(Total material balance)	(A.4a)
	$y_4\dot{m}_4 = x_5\dot{m}_5 + y_6\dot{m}_6$	(Refrigerant material balance)	(A.4b)
	$y_6 = \begin{cases} 1 & \text{, if } T_6 \le T_{sat,refr}(p_{sys}) \\ f_{dew}(T_6, p_{sys}) & \text{, otherwise.} \end{cases}$	(Refrigerant purity)	(A.4c)
	$\dot{m}_4\hat{h}_{V,4} = \dot{m}_5\hat{h}_{L,5} + \dot{m}_6\hat{h}_{V,6} + \dot{Q}_{rect}$	(Energy balance)	(A.4d)
Condenser	$\dot{m}_6 = \dot{m}_{L,7} + \dot{m}_{V,7}$	(Total material balance)	(A.5a)
	$y_6\dot{m}_6 = x_7\dot{m}_{L,7} + y_7\dot{m}_{V,7}$	(Refrigerant material balance)	(A.5b)
	$\{x_7, y_7\} = f(T_7, p_{sys}, y_6)$	(VLE)	(A.5c)
	$\dot{m}_6\hat{h}_{V,6} = \dot{m}_{L,7}\hat{h}_{L,7} + \dot{m}_{V,7}\hat{h}_{V,7} + \dot{Q}_{cond}$	(Energy balance)	(A.5d)
Expansion	$\dot{m}_g = \dot{m}_{V,9}\left(\frac{p_{sys}-p_9}{p_9}\right)\frac{MW_g}{MW_{V,9}}$	(Dalton's law)	(A.6a)
	$p_9 = \begin{cases} p^{sat}_{refr}(T_9) & \text{, if } y_6 = 1 \\ p_{bub}(T_9, x_9) & \text{, otherwise} \end{cases}$	(Expansion pressure)	(A.6b)
	$\dot{m}_{L,7} = \dot{m}_{L,9} + \dot{m}_{V,9}$	(Total material balance)	(A.6c)
	$x_7\dot{m}_{L,7} = x_9\dot{m}_{L,9} + y_9\dot{m}_{V,9}$	(Refrigerant material balance)	(A.6d)
	$\dot{m}_{L,7}\hat{h}_{9'} + \dot{m}_g\int_{T_9}^{T_{9'}}\hat{c}^{ig}_{p,g}(T)\,dT = \dot{m}_{L,9}\hat{h}_{L,9} + \dot{m}_{V,9}\hat{h}_{V,9}$	(Energy balance)	(A.6e)
Evaporator	$p_{10} = \begin{cases} p_{10,max} & \text{, if } p_{10} \ge p_{10,max} \\ \frac{\dot{m}_{V,10}/MW_{V,10}}{\dot{m}_{V,10}/MW_{V,10}+\dot{m}_g/MW_g}p_{sys} & \text{, otherwise} \end{cases}$	(Evaporator pressure)	(A.7a)
	$\dot{m}_{L,7}\hat{h}_{L,7} + \dot{Q}_{evap} = \dot{m}_{V,10}\hat{h}_{V,10} + \dot{m}_{L,10}\hat{h}_{L,10} + \dot{m}_g\int_{T_{s,g}}^{T_{10}}\hat{c}^{ig}_{p,g}(T)\,dT$	(Energy balance)	(A.7b)
	$\dot{m}_{L,7} = \dot{m}_{L,10} + \dot{m}_{V,10}$	(Total material balance)	(A.7c)
	$x_7\dot{m}_{L,7} = x_{10}\dot{m}_{L,10} + y_{10}\dot{m}_{V,10}$	(Refrigerant material balance)	(A.7d)
Absorber	$\dot{m}_{V,10}\hat{h}_{V,10} + \dot{m}_{V,7}\hat{h}_{V,7} + \dot{m}_8\hat{h}_{L,8} + \dot{m}_g\int_{T_{s,g}}^{T_{10}}\hat{c}^{ig}_{p,g}(T)\,dT = \dot{m}_{11}\hat{h}_{L,11} + \dot{Q}_{abs}$	(Energy balance)	(A.8)
Solution heat	$\dot{m}_{rs}(\hat{h}_{L,11} - \hat{h}_1) + \dot{m}_8[\hat{h}(T_{ws,in}, p_{sys}, x_8) - \hat{h}_{L,8}] = 0$	(Energy balance)	(A.9a)
Exchanger	$x_8 = x_{ws} = (x_3\dot{m}_3 + x_5\dot{m}_5)/(\dot{m}_3 + \dot{m}_5)$	(Refrigerant material balance)	(A.9b)
	$\dot{m}_8 = (\dot{m}_3 + \dot{m}_5)$, $\dot{m}_{11} = \dot{m}_1$	(Total material balance)	(A.9c)

CRediT authorship contribution statement

Asmaa A. Harraz: Writing – review & editing, Writing – original draft, Validation, Methodology, Formal analysis, Conceptualization. **Andrew J. Haslam:** Writing – review & editing, Methodology, Conceptualization. **Niall Mac Dowell:** Writing – review & editing, Supervision, Methodology, Conceptualization. **Christos N. Markides:** Writing – review & editing, Supervision, Resources, Project administration, Methodology, Conceptualization.

Declaration of competing interest

The authors declare that they have no known competing financial interests or personal relationships that could have appeared to influence the work reported in this paper.

Acknowledgements

This work was supported by an Institutional Links grant, ID 352350650, under the Newton-Mosharafa Fund partnership. The grant was funded by the UK Department for Business, Energy and Industrial Strategy (BEIS) and the Science, Technology, and Innovation Funding Authority (STDF), Egypt, and delivered by the British Council. For further information, please visit the Newton Fund page on the British Council website. The work was also supported by the UK Engineering and Physical Sciences Research Council (EPSRC) [grant numbers EP/P030920/1, and EP/P004709/1]. Asmaa A. Harraz received a full PhD Newton-Mosharafa scholarship from the Ministry of Higher Education of the Arab Republic of Egypt and the British Council. The authors would also like to thank UK company Solar Polar Ltd. Data supporting this publication can be obtained on request from cep-lab@imperial.ac.uk. For the purpose of Open Access, the authors have applied a CC BY public copyright licence to any Author Accepted Manuscript version arising from this submission.

Appendix. DAR system model

A fundamental thermodynamic model for DAR modules is adopted based on the conservation of energy and mass, avoiding – whenever possible – the use of system-specific correlations. This ensures transferability to different DAR modules and working fluids. The presented model is summarised in Table A.1. As any refrigeration system, the thermodynamic performance of DAR is indicated by its coefficient of performance, COP, given by:

$$COP = \frac{\dot{Q}_{evap}}{\dot{Q}_{gen}}. \quad (A.1)$$

Data availability

Data will be made available on request.

References

[1] IEA. The future of cooling: Opportunities for energy-efficient air conditioning. 2018, [Online], available from https://www.iea.org/reports/the-future-of-cooling, [Last Accessed on: 1 August 2024].

[2] N'Tsoukpoe KE, Yamegueu D, Bassole J. Solar sorption refrigeration in Africa. Renew Sustain Energy Rev 2014;35:318–35. http://dx.doi.org/10.1016/j.rser.2014.04.030.

[3] Platen BCV, Munters CG. Refrigeration. 1928, US-Patent 1678277.

[4] Platen BCV, Munters CG. Refrigerator. 1928, US-Patent 1685764.

[5] Rodríguez-Muñoz JL, Belman-Flores JM. Review of diffusion-absorption refrigeration technologies. Renew Sustain Energy Rev 2014;30:145–53. http://dx.doi.org/10.1016/j.rser.2013.09.019.

[6] Rademacher R, Herold KE, Radermacher R, Klein SA. Absorbtion chillers and heat pumps. CRC; 2016, http://dx.doi.org/10.1201/b19625.

[7] Zohar A, Jelinek M, Levy A, Borde I. The influence of the generator and bubble pump configuration on the performance of diffusion absorption refrigeration (DAR) system. Int J Refrig 2008;31(6):962–9. http://dx.doi.org/10.1016/j.ijrefrig.2008.01.009.

[8] Kim G, Choi HW, Lee G, Lee JS, Kang YT. Experimental study on diffusion absorption refrigeration systems with low GWP refrigerants. Energy 2020;201:117626. http://dx.doi.org/10.1016/j.energy.2020.117626.

[9] Najjaran A, Harraz AA, Freeman J, Mac Dowell N, Markides CN. Numerical and experimental investigation of diffusion absorption refrigeration systems for use with low-temperature heat sources. In: Teixeira JC, editor. ECOS 2018: Proceedings of the 31st International Conference on Efficiency, Cost, Optimization, Simulation and Environmental Impact of Energy Systems, Guimarães, Portugal. 2018, p. 323.

[10] NIST/TRC Web Thermo Tables (WTT).

[11] Zohar A, Jelinek M, Levy A, Borde I. Numerical investigation of a diffusion absorption refrigeration cycle. Int J Refrig 2005;28(4):515–25. http://dx.doi.org/10.1016/j.ijrefrig.2004.11.003.

[12] Freeman J, Najjaran-Kheirabadi A, Edwards R, Reid M, Hall R, Ramos A, et al. Testing and simulation of a solar diffusion-absorption refrigeration system for low-cost solar cooling in India. In: ISES solar world congress. 2017.

[13] Najjaran A, Freeman J, Ramos A, Markides CN. Experimental performance analysis of an ammonia-water diffusion absorption refrigeration cycle. In: Mayer JP, editor. 13th international conference on heat transfer, fluid mechanics and thermodynamics, Portorož, Slovenia. 2017, p. 951–5.

[14] Najjaran A, Harraz AA, Sapin P, Wang K, Markides CN. Experimental investigation on the start-up time of a small-scale diffusion absorption refrigeration (DAR) unit. In: 14th international conference on heat transfer, fluid mechanics and thermodynamics, Wicklow, Ireland. 2019.

[15] Najjaran A, Freeman J, Ramos A, Markides CN. Experimental investigation of an ammonia-water-hydrogen diffusion absorption refrigerator. Appl Energy 2019;256. http://dx.doi.org/10.1016/j.apenergy.2019.113899.

[16] Srikhirin P, Aphornratana S, Chungpaibulpatana S. A review of absorption refrigeration technologies. Renew Sustain Energy Rev 2001;5(4):343–72. http://dx.doi.org/10.1016/S1364-0321(01)00003-X.

[17] Ezzine NB, Garma R, Bellagi A. A numerical investigation of a diffusion-absorption refrigeration cycle based on R124-DMAC mixture for solar cooling. Energy 2010;35(5):1874–83. http://dx.doi.org/10.1016/j.energy.2009.12.032.

[18] Wang H. A new style solar-driven diffusion absorption refrigerator and its operating characteristics. Energy Procedia 2012;18:681–92. http://dx.doi.org/10.1016/j.egypro.2012.05.083.

[19] Freeman J, Ramos A, Mac Dowell N, Markides CN. An experimentally validated model of a solar-cooling system based on an ammonia-water diffusion-absorption cycle. In: The 8th international conference on applied energy – ICAE2016, Beijing, China. 2016.

[20] Freeman J. Solar-thermal combined energy systems for distributed small-scale applications [Ph.D. thesis], London, UK: Imperial College London; 2017.

[21] Özbaş E. Experimental study of diffusion absorption refrigeration systems using solar energy. J Polytech 2018;21(2):291–7. http://dx.doi.org/10.2339/politeknik.385931.

[22] Schmid F, Bierling B, Spindler K. Development of a solar-driven diffusion absorption chiller. Sol Energy 2019;177:483–93. http://dx.doi.org/10.1016/J.SOLENER.2018.11.040.

[23] Ramos A, Guarracino I, Mellor A, Alonso-Álvarez D, Childs P, Ekins-daukes N, et al. Briefing paper no 22: solar-thermal and hybrid photovoltaic-thermal systems for revewable heating. Imperial College London, Grantham Institute; 2017.

[24] Acuña A, Lara F, Velázquez N, Cerezo J. Optimum generator temperature to couple different diffusion absorption solar cooling systems. Energy Econ 2014;45:128–35. http://dx.doi.org/10.1016/j.ijrefrig.2014.05.016.

[25] Acuña A, Velázquez N, Sauceda D, Rosales P, Suastegui A, Ortiz A. Influence of a compound parabolic concentrator in the performance of a solar diffusion absorption cooling system. Appl Therm Eng 2016;102:1374–83. http://dx.doi.org/10.1016/j.applthermaleng.2016.03.061.

[26] Harraz AA, Freeman J, Wang K, Mac Dowell N, Markides CN. Diffusion-absorption refrigeration cycle simulations in gPROMS using SAFT-γ Mie. Energy Procedia 2019;158:2360–5. http://dx.doi.org/10.1016/j.egypro.2019.01.284.

[27] Harraz AA. Computer-aided molecular and system design of diffusion absorption solar-cooling systems. [Ph.D. thesis], London, UK: Imperial College London; 2022.

[28] Stegou-Sagia A. A computational method for the methyl amine/H_2 gas mixture concentrations in methyl amine/H_2O/H_2 absorption refrigeration units. Appl Therm Eng 1996;16(8):707–18. http://dx.doi.org/10.1016/1359-4311(95)00077-1.

[29] Zohar A, Jelinek M, Levy A, Borde I. Performance of diffusion absorption refrigeration cycle with organic working fluids. Int J Refrig 2009;32(6):1241–6. http://dx.doi.org/10.1016/j.ijrefrig.2009.01.010.

[30] Wang Q, Gong L, Wang J, Sun T, Cui K, Chen G. A numerical investigation of a diffusion absorption refrigerator operating with the binary refrigerant for low temperature applications. Appl Therm Eng 2011;31(10):1763–9. http://dx.doi.org/10.1016/j.applthermaleng.2011.02.021.

[31] Ben Ezzine N, Garma R, Bellagi A. Experimental and numerical investigation on absorption-diffusion refrigeration machine based on light hydrocarbons. In: Proceedings of SEBUA-12 ICHMT international symposium on sustainable energy in buildings and urban areas. 2012, p. 329–34.

[32] Sayadi Z, Thameur B, Bourouis M, Bellagi A, Thameur NB, Bourouis M, et al. Performance optimization of solar driven small-cooled absorption–diffusion chiller working with light hydrocarbons. Energy Convers Manage 2013;74:299–307. http://dx.doi.org/10.1016/j.enconman.2013.05.029.

[33] Dardour H, Cézac P, Reneaume J-M, Bourouis M, Bellagi A. Numerical investigation of an absorption-diffusion cooling machine using C_3H_8/C_9H_{20} as binary working fluid. Oil Gas Sci Technol – Rev D' IFP Energies Nouv 2013;68(2):249–54. http://dx.doi.org/10.2516/ogst/2012086.

[34] Long Z, Luo Y, Li H, Bu X, Ma W. Performance analysis of a diffusion absorption refrigeration cycle working with TFE–TEGDME mixture. Energy Build 2013;58:86–92. http://dx.doi.org/10.1016/j.enbuild.2012.12.003.

[35] Mazouz S, Mansouri R, Bellagi A. Experimental and thermodynamic investigation of an ammonia/water diffusion absorption machine. Int J Refrig 2014;45:83–91. http://dx.doi.org/10.1016/j.ijrefrig.2014.06.002.

[36] Agostini B, Agostini F, Habert M. Modeling of a Von Platen-Munters diffusion absorption refrigeration cycle. J Phys: Conf Ser 2016;745:032053. http://dx.doi.org/10.1088/1742-6596/745/3/032053.

[37] Zhang B, Chen W, Sun Q, Miao Z. Numerical evaluation of thermal performances of diffusion–absorption refrigeration using 1,3-dimethylimidazolylium dimethylphosphate/methanol/helium as working fluid. Energy Convers Manage 2017;152:201–13. http://dx.doi.org/10.1016/j.enconman.2017.09.048.

[38] Wankhede SV, Hole JA, Patil BL. Performance of tetrafluoroethane (R134a)-dimethyl formamide (DMF) diffusion absorption air cooling system with variable power input. Int J Ambient Energy 2020;1–7. http://dx.doi.org/10.1080/01430750.2020.1722225.

[39] Li H, Lin P, Du S, Wang L. Modelling and thermodynamic analysis of a hot-cold conversion pipe using R134a-DMF-He as the working pair. J Therm Sci 2021;30(1):64–75. http://dx.doi.org/10.1007/s11630-020-1243-0.

[40] Lee G, Choi HW, Kang YT. Cycle performance analysis and experimental validation of a novel diffusion absorption refrigeration system using R600a/n-octane. Energy 2021;217:119328. http://dx.doi.org/10.1016/j.energy.2020.119328.

[41] Choi HW, Lee JW, Kang YT. Experimental study on diffusion absorption refrigerator achieving 0.2 coefficient of performance using low global warming potential refrigerant and low-grade heat source. Appl Therm Eng 2022;201:117803. http://dx.doi.org/10.1016/j.applthermaleng.2021.117803.

[42] Harraz AA, Najjaran A, Sacks R, Freeman J, Olympios AV, Mac Dowell N, et al. Experimentally validated simulations of a diffusion absorption refrigeration system. In: ECOS 2019: Proceedings of the 32nd international conference on efficiency, cost, optimization, simulation and environmental impact of energy systems, Wroclaw, Poland. 2019.

[43] Austin ND, Sahinidis NV, Trahan DW. Computer-aided molecular design: An introduction and review of tools. Appl Solut Tech Chem Eng Res Des 2016;116:2–26. http://dx.doi.org/10.1016/j.cherd.2016.10.014.

[44] Ng LY, Chong FK, Chemmangattuvalappil NG. Challenges and opportunities in computer-aided molecular design. Comput Chem Eng 2015;81:115–29. http://dx.doi.org/10.1016/j.compchemeng.2015.03.009.

[45] Seider WD, Lewin DR, Seader JD, Widagdo S, Gani R, NG KM. Product and process design principles: synthesis, analysis, and evaluation. 4th ed. John Wiley & Sons Inc.; 2017.

[46] Achenie L, Venkatasubramanian V, Gani R. Computer aided molecular design: theory and practice. 1st ed. Elsevier; 2002.

[47] Kernen M, Lee LL, Perez-Blanco H. A computer-aided molecular design of fluids that optimize absorption cycle COP. J Energy Resour Technol 1995;117(2):156–60. http://dx.doi.org/10.1115/1.2835332.

[48] Khetib Y, Larkeche O, Meniai A-H, Radwan A. Group contribution concept for computer-aided design of working fluids for refrigeration machines. Chem Eng Technol 2013;36(11):1924–34. http://dx.doi.org/10.1002/ceat.201300058.

[49] Khetib Y, Meniai A-H, Gari A, Sedraoui K. Refrigerants design for an absorption refrigeration machine using group contribution methods. Chem Eng Commun 2021;210(4):471–89. http://dx.doi.org/10.1080/00986445.2021.1948409.

[50] Churi N, Achenie LEK. Novel mathematical programming model for computer aided molecular design. Ind Eng Chem Res 1996;35(10):3788–94. http://dx.doi.org/10.1021/ie9601920.

[51] Churi N, Achenie L. On the use of a mixed integer non-linear programming model for refrigerant design. Int Trans Oper Res 1997;4(1):45–54. http://dx.doi.org/10.1111/j.1475-3995.1997.tb00061.x.

[52] Duvedi A, Achenie L. On the design of environmentally benign refrigerant mixtures: a mathematical programming approach. Comput Chem Eng 1997;21(8):915–23. http://dx.doi.org/10.1016/S0098-1354(96)00310-9.

[53] Louaer I, Meniai A, Larkeche O, Bencheikh-Lehocine M. Computer-aided design and test of new refrigerants for an absorption cycle using group contribution methods. Desalination 2007;206(1):620–32. http://dx.doi.org/10.1016/j.desal.2006.04.067.

[54] Tora EA-H. Computer-aided design and simulation of working fluid pairs for absorption refrigerators. Int J Sci Eng Res 2013;4(4):1306–10.

[55] Schilling J, Lampe M, Gross J, Bardow A. 1-stage CoMT-CAMD: An approach for integrated design of ORC process and working fluid using PC-SAFT. Chem Eng Sci 2017;159:217–30. http://dx.doi.org/10.1016/j.ces.2016.04.048, iCAMD – Integrating Computer-Aided Molecular Design into Product and Process Design.

[56] Schilling J, Tillmanns D, Lampe M, Hopp M, Gross J, Bardow A. From molecules to dollars: integrating molecular design into thermo-economic process design using consistent thermodynamic modeling. Mol Syst Des Eng 2017;2:301–20. http://dx.doi.org/10.1039/C7ME00026J.

[57] White MT, Oyewunmi OA, Haslam AJ, Markides CN. Industrial waste-heat recovery through integrated computer-aided working-fluid and ORC system optimisation using SAFT-γ Mie. Energy Convers Manage 2017;150:851–69. http://dx.doi.org/10.1016/j.enconman.2017.03.048.

[58] van Kleef LM, Oyewunmi OA, Markides CN. Multi-objective thermo-economic optimization of Organic Rankine Cycle (ORC) power systems in waste-heat recovery applications using computer-aided molecular design techniques. Appl Energy 2019;251:112513. http://dx.doi.org/10.1016/j.apenergy.2019.01.071.

[59] Oyewunmi OA. Heat recovery and conversion technologies with organic fluid cycles: optimal working fluid and system design. [Ph.D. thesis], London, UK: Imperial College London; 2018.

[60] Papadopoulos AI, Kyriakides A-S, Seferlis P, Hassan I. Integrated design of working fluid mixtures and absorption refrigeration cycles. Front Chem Eng 2021;3. http://dx.doi.org/10.3389/fceng.2021.622998.

[61] Churi N, Achenie LE. The optimal design of refrigerant mixtures for a two-evaporator refrigeration system. Comput Chem Eng 1997;21:S349–54. http://dx.doi.org/10.1016/S0098-1354(97)87526-6, supplement to Computers and Chemical Engineering.

[62] Larkeche O, Meniai A-H, Cachot T. Modelling the absorption refrigeration cycle using partially miscible working fluids by group contribution methods. Mol Phys 2012;110(11–12):1305–16. http://dx.doi.org/10.1080/00268976.2012.666275.

[63] Dufal S, Lafitte T, Galindo A, Jackson G, Haslam AJ. Developing intermolecular-potential models for use with the SAFT-VR Mie equation of state. AIChE J 2015;61(9):2891–912. http://dx.doi.org/10.1002/aic.14808.

[64] Papaioannou V, Lafitte T, no CA, Adjiman CS, Jackson G, Müller EA, Galindo A. Group contribution methodology based on the statistical associating fluid theory for heteronuclear molecules formed from mie segments. J Chem Phys 2014;140(5):054107. http://dx.doi.org/10.1063/1.4851455.

[65] Starace G, De Pascalis L. An advanced analytical model of the diffusion absorption refrigerator cycle. Int J Refrig 2012;35(3):605–12. http://dx.doi.org/10.1016/j.ijrefrig.2011.11.007.

[66] Mansouri R, Bourouis M, Bellagi A. Steady state investigations of a commercial diffusion-absorption refrigerator: Experimental study and numerical simulations. Appl Therm Eng 2018;129:725–34. http://dx.doi.org/10.1016/j.applthermaleng.2017.10.010.

[67] Chaves F, Moreira M, Koury R, Machado L, Cortez M. Experimental study and modeling within validation of a diffusion absorption refrigerator. Int J Refrig 2019;101:136–47. http://dx.doi.org/10.1016/j.ijrefrig.2019.01.019.

[68] Pérez-García V, Rodríguez-Muñoz J, Belman-Flores J, Rubio-Maya C, Ramírez-Minguela J. Theoretical modeling and experimental validation of a small capacity diffusion-absorption refrigerator. Int J Refrig 2019;104:302–10. http://dx.doi.org/10.1016/j.ijrefrig.2019.05.014.

[69] Zohar A, Jelinek M, Levy A, Borde I. The influence of diffusion absorption refrigeration cycle configuration on the performance. Appl Therm Eng 2007;27(13):2213–9. http://dx.doi.org/10.1016/j.applthermaleng.2005.07.025.

[70] Starace G, De Pascalis L. An enhanced model for the design of diffusion absorption refrigerators. Int J Refrig 2013;36(5):1495–503. http://dx.doi.org/10.1016/j.ijrefrig.2013.02.016.

[71] Mejbri K, Bellagi A. Modelling of the thermodynamic properties of the water-ammonia mixture by three different approaches. Int J Refrig 2006;29(2):211–8. http://dx.doi.org/10.1016/j.ijrefrig.2005.06.002.

[72] Taieb A, Mejbri K, Bellagi A. Theoretical analysis of a diffusion-absorption refrigerator. Int J Hydrog Energy 2016;41(32):14293–301. http://dx.doi.org/10.1016/j.ijhydene.2016.06.180.

[73] Taieb A, Mejbri K, Bellagi A. Detailed thermodynamic analysis of a diffusion-absorption refrigeration cycle. Energy 2016;115:418–34. http://dx.doi.org/10.1016/j.energy.2016.09.002.

[74] Pátek J, Klomfar J. Simple functions for fast calculations of selected thermodynamic properties of the ammonia-water system. Int J Refrig 1995;18(4):228–34. http://dx.doi.org/10.1016/0140-7007(95)00006-W.

[75] Gani R, Nielsen B, Fredenslund A. A group contribution approach to computer-aided molecular design. AIChE J 1991;37(9):1318–32. http://dx.doi.org/10.1002/aic.690370905.

[76] Joback KG, Reid R. Estimation of pure-component properties from group-contributions. Chem Eng Commun 1987;57(1–6):233–43. http://dx.doi.org/10.1080/00986448708960487.

[77] Fredenslund A, Jones RL, Prausnitz JM. Group-contribution estimation of activity coefficients in nonideal liquid mixtures. AIChE J 1975;21(6):1086–99. http://dx.doi.org/10.1002/aic.690210607.

[78] Fredenslund A, Gmehling J, Rasmussen P. Vapor-liquid equilibria using UNIFAC: A group-contribution method. Amsterdam: Elsevier; 1977.

[79] Weidlich U, Gmehling J. A modified UNIFAC model. 1. Prediction of VLE, h^E and γ^∞. Ind Eng Chem Res 1987;26(7):1372–81. http://dx.doi.org/10.1021/ie00067a018.

[80] Chapman WG, Gubbins KE, Jackson G, Radosz M. SAFT: Equation-of-state solution model for associating fluids. Fluid Phase Equilib 1989;52:31–8. http://dx.doi.org/10.1016/0378-3812(89)80308-5.

[81] Chapman WG, Gubbins KE, Jackson G, Radosz M. New reference equation of state for associating liquids. Ind Eng Chem Res 1990;29(8):1709–21. http://dx.doi.org/10.1021/ie00104a021.

[82] Wertheim MS. Fluids with highly directional attractive forces: I. Statistical thermodynamics. J Stat Phys 1984;35(1–2):19–34.

[83] Wertheim MS. Fluids with highly directional attractive forces: II. Thermodynamic perturbation theory and integral equations. J Stat Phys 1984;35(1–2):35–47.

[84] Wertheim MS. Fluids with highly directional attractive forces: III. Multiple attraction sites. J Stat Phys 1986;42(3–4):459–76.

[85] Wertheim MS. Fluids with highly directional attractive forces: IV. Equilibrium polymerization. J Stat Phys 1986;42(3–4):477–92.

[86] Dufal S, Papaioannou V, Sadeqzadeh M, Pogiatzis T, Chremos A, Adjiman CS, et al. Prediction of thermodynamic properties and phase behavior of fluids and mixtures with the SAFT-γ Mie group-contribution equation of state. J Chem Eng Data 2014;59(10):3272–88. http://dx.doi.org/10.1021/je500248h.

[87] Papaioannou V, Calado F, Lafitte T, Dufal S, Sadeqzadeh M, Jackson G, et al. Application of the SAFT-γ Mie group contribution equation of state to fluids of relevance to the oil and gas industry. Fluid Phase Equilib 2016;416:104–19. http://dx.doi.org/10.1016/J.FLUID.2015.12.041.

[88] Haslam AJ, González-Pérez A, Lecce SD, Khalit SH, Perdomo FA, Kournopoulos S, et al. Expanding the applications of the SAFT-γ Mie group-contribution equation of state: Prediction of thermodynamic properties and phase behavior of mixtures. J Chem Eng Data 2020;65(12):5862–90. http://dx.doi.org/10.1021/ACS.JCED.0C00746.

[89] Hutacharoen P, Dufal S, Papaioannou V, Shanker RM, Adjiman CS, Jackson G, et al. Predicting the solvation of organic compounds in aqueous environments: From alkanes and alcohols to pharmaceuticals. Ind Eng Chem Res 2017;56(38):10856–76. http://dx.doi.org/10.1021/acs.iecr.7b00899.

[90] Di Lecce S, Lazarou G, Khalit SH, Adjiman CS, Jackson G, Galindo A, et al. Modelling and prediction of the thermophysical properties of aqueous mixtures of choline geranate and geranic acid (CAGE) using SAFT-γ Mie. RSC Adv 2019;9:38017–31. http://dx.doi.org/10.1039/C9RA07057E.

[91] Bagga A, Teoh M. Thermodynamic modelling of ammonia and ammonia-water mixture using SAFT-VR Mie [Master's thesis], London, UK: Imperial College London; 2017.

[92] Rowlinson JS, Swinton FL. Liquids and liquid mixtures. 3rd ed. Butterworths & Co; 1982.

[93] Conde Engineering M. Thermophysical properties of NH_3+H_2O mixtures for the industrial design of absorption refrigeration equipment. Tech. rep., Zurich: M. Conde Engineering; 2006, last updated 2014.

[94] Poling BE, Prausnitz JM, O'Connell JP. The properties of gases and liquids. McGraw-Hill Education; 2001.

[95] Sastri SRS, Rao KK. A simple method to predict surface tension of organic liquids. Chem Eng J Biochem Eng J 1995;59(2):181–6. http://dx.doi.org/10.1016/0923-0467(94)02946-6.

[96] IAPWS. Revised release on surface tension of ordinary water substance. Tech. rep., International Association of Pure Water and Steam; 2014.

[97] Rattner AS, Garimella S. Low-source-temperature diffusion absorption refrigeration. Part I: Modeling and cycle analysis. Int J Refrig 2016;65:287–311. http://dx.doi.org/10.1016/j.ijrefrig.2015.10.010.

[98] Freeman J. Towards an off-design model of a diffusion absorption refrigeration (DAR) system for solar-cooling applications. Tech. rep., London, UK: Imperial College London; 2018.

[99] Hewitt GF, Shires GL, Bott TR. Process heat transfer. CRC Press; 1994.
[100] RV cooling unit warehouse [online]. 2024, https://rvcoolingunit.com/. [Last Accessed On: 01 August 2024].
[101] HM Revenue & Customs. Guidance: Average for the year to 31 2022. 2022.
[102] Chemical Engineerin. The Chemical Engineering Plant Cost Index. Chem Eng Essentials the CPI Prof 2023;130(1):48.
[103] Levenberg K. A method for the solution of certain non-linear problems in least squares. Quart Appl Math 1944;2(2):164–8.
[104] Marquardt DW. An algorithm for least-squares estimation of nonlinear parameters. J Soc Ind Appl Math 1963;11(2):431–41. http://dx.doi.org/10.1137/0111030.
[105] Taitel Y, Bornea D, Dukler AE. Modelling flow pattern transitions for steady upward gas-liquid flow in vertical tubes. AIChE J 1980;26(3):345–54. http://dx.doi.org/10.1002/aic.690260304.
[106] Odele O, Macchietto S. Computer aided molecular design: a novel method for optimal solvent selection. Fluid Phase Equilib 1993;82:47–54. http://dx.doi.org/10.1016/0378-3812(93)87127-M.
[107] Markides CN, Bardow A, De Paepe M, De Servi C, Haslam JGAJ, Lecompte S, et al. Working fluid and system optimisation of Organic Rankine Cycles via computer-aided molecular design: A review. Prog Energy Combust Sci 2025;107:101201. http://dx.doi.org/10.1016/j.pecs.2024.101201.
[108] Papadopoulos AI, Perdomo FA, Tzirakis F, Shavalieva G, Tsivintzelis I, Kazepidis P, et al. Molecular engineering of sustainable phase-change solvents: From digital design to scaling-up for CO_2 capture. Chem Eng J 2021;420:127624. http://dx.doi.org/10.1016/j.cej.2020.127624.
[109] Albahri TA, George RS. Artificial neural network investigation of the structural group contribution method for predicting pure components auto ignition temperature. Ind Eng Chem Res 2003;42(22):5708–14. http://dx.doi.org/10.1021/ie0300373.
[110] Kondo S, Urano Y, Tokuhashi K, Takahashi A, Tanaka K. Prediction of flammability of gases by using Γ-number analysis. J Hazard Mater 2001;82(2):113–28. http://dx.doi.org/10.1016/S0304-3894(00)00358-7.
[111] Hukkerikar AS, Kalakul S, Sarup B, Young DM, Sin G, Gani R. Estimation of environment-related properties of chemicals for design of sustainable processes: Development of group-contribution+ (GC+) property models and uncertainty analysis. J Chem Inf Model 2012;52(11):2823–39. http://dx.doi.org/10.1021/ci300350r, pMID: 23039255, arXiv:10.1021/ci300350r.
[112] Freeman J, Markides CN. A solar diffusion-absorption refrigeration system for off-grid cold-chain provision. Part I: Model development and experimental calibration. Renew Energy 2024;230:120718. http://dx.doi.org/10.1016/j.renene.2024.120718.
[113] Freeman J, Markides CN. A solar diffusion-absorption refrigeration system for off-grid cold-chain provision, Part II: System simulation and assessment of performance. Renew Energy 2024;230:120717. http://dx.doi.org/10.1016/j.renene.2024.120717.
[114] Dutta S. Optimization in chemical engineering. Cambridge University Press; 2016.
[115] Lee YS, Graham EJ, Galindo A, Jackson G, Adjiman CS. A comparative study of multi-objective optimization methodologies for molecular and process design. Comput Chem Eng 2020;136:106802. http://dx.doi.org/10.1016/j.compchemeng.2020.106802.
[116] Messac A, Ismail-Yahaya A, Mattson C. The normalized normal constraint method for generating the pareto frontier. Struct Multidiscip Optim 2003;25(2):86–98. http://dx.doi.org/10.1007/s00158-002-0276-1.
[117] PSE: gPROMS - Home - Process Systems Enterprise [online]. 2024, https://www.siemens.com/global/en/products/automation/industry-software/gproms-digital-process-design-and-operations.html. [Last Accessed On: 01 August 2024].
[118] Sobol' IM, Asotsky D, Kreinin A, Kucherenko S. Construction and comparison of high-dimensional sobol' generators. Wilmott 2011;2011(56):64–79. http://dx.doi.org/10.1002/wilm.10056.
[119] Viswanathan J, Grossmann IE. A combined penalty function and outer-approximation method for MINLP optimization. Comput Chem Eng 1990;14(7):769–82. http://dx.doi.org/10.1016/0098-1354(90)87085-4.
[120] Berkelaar M, Dirks J, Eikland K, Notebaert P, Ebert J, Gourvest H. lpsolve: interface to 'lp_solve'v. 5.5 to solve linear/integer programs. R package version 5.6. 13. 2015.
[121] Najjaran A. Diffusion absorption refrigeration systems for thermally-driven cooling from low-temperature heat sources. [Ph.D. thesis], London, UK: Imperial College London; 2020.
[122] Boman DB, Hoysall DC, Staedter MA, Goyal A, Ponkala MJ, Garimella S. A method for comparison of absorption heat pump working pairs. Int J Refrig 2017;77:149–75. http://dx.doi.org/10.1016/j.ijrefrig.2017.02.023.
[123] PubChem [Internet]. Bethesda (MD): National Library of Medicine (US), National Center for Biotechnology information. 2004, PubChem Compound LCSS for CID 7853, Allylamine, https://pubchem.ncbi.nlm.nih.gov/compound/7853#datasheet=LCSS. [Last Accessed On: 1 August 2024].